8-2007

Carbon Nanomaterials in Biological Systems

Sijie Lin
Clemson University, slin@clemson.edu

CARBON NANOMATERIALS IN BIOLOGICAL SYSTEMS

A Thesis
Presented to
the Graduate School of
Clemson University

In Partial Fulfillment
of the Requirements for the Degree
Master of Science
Polymer and Fiber Science

---

by
Sijie Lin
August 2007

Accepted by:
Dr. Pu-Chun Ke, Committee Chair
Dr. Jian Luo
Dr. Konstantin Kornev

ABSTRACT

This thesis intends to present, from the biophysical viewpoint, my study on understanding carbon nanomaterials in biological and environmental systems. Carbon nanotubes and fullerenes represent a major family of carbon nanoparticles which possess distinct electrical, optical and mechanical properties. However, the major hurdle for making carbon nanomaterials bioavailable lies in their tendency toward bundling, driven by hydrophobic interaction, van der Waals force, and pi-stacking. To overcome this problem, we used non-covalent binding of zwitterionic lysophopholipids (LPL) onto the external surfaces of single-walled carbon nanotubes (SWNTs). This method affords superior SWNT solubility in aqueous solution. The stability of SWNT-LPL complex has been found to be dependent on the pH of the solvent, but independent of solvent temperature. Based on this method, the translocation of rhodamine-lysophosphoethanolamine-SWNT (Rd-LPE-SWNT) complex across cell membranes, as well as the dissociation of Rd-LPE from SWNTs in the cellular environment was detected using the technique of fluorescence resonance energy transfer (FRET). Towards understanding the environmental impact of carbon nanomaterials, we have studied the biomodification of SWNT-lyso-phosphatidylcholine (SWNT-LPC) by aquatic organism Daphnia magna. Through normal feeding behavior, Daphnia magna ingested SWNT-LPC and stripped out the lipids as food source. SWNTs rebundled inside the guts of daphnia and were excreted into the water column. Acute toxicity was observed only in the highest test concentrations of 0.5 mg/L under starvation conditions. Regarding fullerenes, C_{70}, the shortest "SWNT", was solubilized in water by gallic acid, a natural anti-oxidant and anticancer agent. The suparmolecular complex of C_{70}-gallic acid, assembled

through pi-stacking, emitted green fluorescence in aqueous solution. Utilizing this optical property, we succeeded in labeling biological systems at cellular, tissue and living organism levels. We have further discovered that the fluorescence of C_{70} is far more resistant to photobleaching than calcein AM, a conventional dye for bioimaging. Using confocal fluorescence microscopy we have obtained the first real-time observation of nanoparticle translocation across cell membranes.

In summary, the objectives of this thesis are:

- Solubilizating SWNT in aqueous solution afforded by different solvating agents, including DOPA, sodium dodecyl sulfate (SDS) and LPC, and testing the stability of the solution at different temperatures, pH and ionic strengths;
- Using SWNT as a transporter for lipid delivery across cell membranes;
- Understanding the fate of SWNT in aquatic organism *Daphnia magna*; and
- Coating C_{70} with gallic acid and utilizing the optical properties of C_{70} for detecting its cell translocation.

The studies documented in this thesis further our understanding of the interactions between carbon nanomaterials and biological and environmental systems. Water soluble carbon nanomaterials enable future field studies in imaging, sensing, drug delivery, nanotoxicity, nanomedicine, and environmental science and engineering.

DEDICATION

This thesis is dedicated to my parents and beloved ones.

ACKNOWLEDGMENTS

I would like to thank many people who have helped and supported me the past two years at Clemson.

My deep appreciation goes to Dr. Pu-Chun Ke. It has been the most fortunate to have Dr. Ke as my advisor. He kindly accepted me as a group member when I first came to Clemson without any support. From him, I have realized what a passionate and devoted researcher I want to become. Dr. Ke taught me the basic theories in biophysics; he guided me through every step in the lab; and he showed me how to logically analyze data and approach the process of paper writing and publication. I feel his excellent scientific research skills and studious working style have strongly influenced me. And I am indebted to him for introducing me to the exciting field of biophysical nanoscience.

Many thanks to my committee members Dr. Jian Luo and Dr. Konstantin Kornev. I have greatly enjoyed fruitful discussions with Dr. Luo several times regarding potential research projects. I am also honored to have Dr. Konev evaluating my thesis.

I also wish to thank Dr. Xi Wang, Dr. Andrew Mount, and Dr. Stephen Klaine for their instructions. Dr. Wang taught me cell culture. Dr. Mount trained me on confocal microscopy. Dr. Klaine brought fruitful collaborations led to our joint paper and more research opportunities.

I would also like to thank my coworkers Jessica Moore, Dr. Qi Lu, Michelle Reid, Karthikeyan Pasupathy, Donovan Jones, An-Hong Cheng, Jun Lin and Marcus Allegood for their selfless help and friendships.

I wish to thank all who have helped me find my place at Clemson.

TABLE OF CONTENTS

Page

LIST OF FIGURES

List of Figures (Continued)

CHAPTER ONE

INTRODUCTION

Single-walled carbon nanotubes (SWNTs) and fullerenes are representatives of carbon nanomaterials and possess unique mechanical, thermal, and electrical properties [1, 2, 3, 4]. These nanomaterials are the backbones for the "bottom-up" approach in nanotechnology [5]. To gain a fundamental understanding of these nanomaterials, this section details the structures of SWNTs and fullerenes, especially, C_{60} and C_{70}, and highlights their applications in biological systems. The principles of fluorescence microscopy and fluorescence resonance energy transfer (FRET), the two major techniques used in my research, will be introduced. The topic of nanotoxicity is discussed to the address the uncertainties over the potential adverse effects of carbon nanomaterials on human health and the environment.

Structures of SWNTs

Solid state carbon has been known to appear in four basic forms: diamond, graphite, non-crystalline structures (such as charcoal), and fullerene molecules, such as C_{60}, which is comprised of 60 carbon atoms clustered in a soccer ball. Carbon nanotubes are the fifth type of solid state carbon discovered by Iijima [6] in the early 90's. The structures of carbon nanotubes can be viewed using electronic microscopy. Based on the number of walls that carbon nanotubes have, they can be divided into single-walled, double-walled, and multi-walled carbon nanotubes (MWNTs). As allotropes of carbon, carbon nanotubes are

composed entirely of sp2 bonds, similar to that of graphite. This bonding is stronger than the sp3 bonds found in diamond, and provides the molecules unique and versatile properties.

The structure of an SWNT can be described as a seamless hollow cylinder formed by rolling a one-atom-thick of graphene sheet [7]. Depending on how the graphene sheet is rolled up, an SWNT may possess different optical activity, mechanical strength, and electrical conductivity of the nanostructure. Usually, a chiral vector is used to describe the structure of the SWNT (Figure 1.1). The integers n and m denote the number of unit vectors along two directions in the honeycomb crystal lattice of graphene. If m=0, the nanotubes are called "zigzag", if n=m, the nanotubes are called "armchair". Otherwise, they are called "chiral" (Figure 1.2) [8]. Take the electrical conductivity for example, for a given (n,m) nanotube, if (n-m) is a multiple of 3, then the nanotube is metallic, otherwise the nanotube is semiconducting.

Since the diameter of an SWNT is ~1 nm and its tube length can be many thousands of times longer, an SWNT is usually considered as a one-dimensional structure. In practice, SWNTs have been produced in various ways, including arc discharge, laser ablation, chemical vapour deposition, and flame synthesis [9, 10, 11, 12].

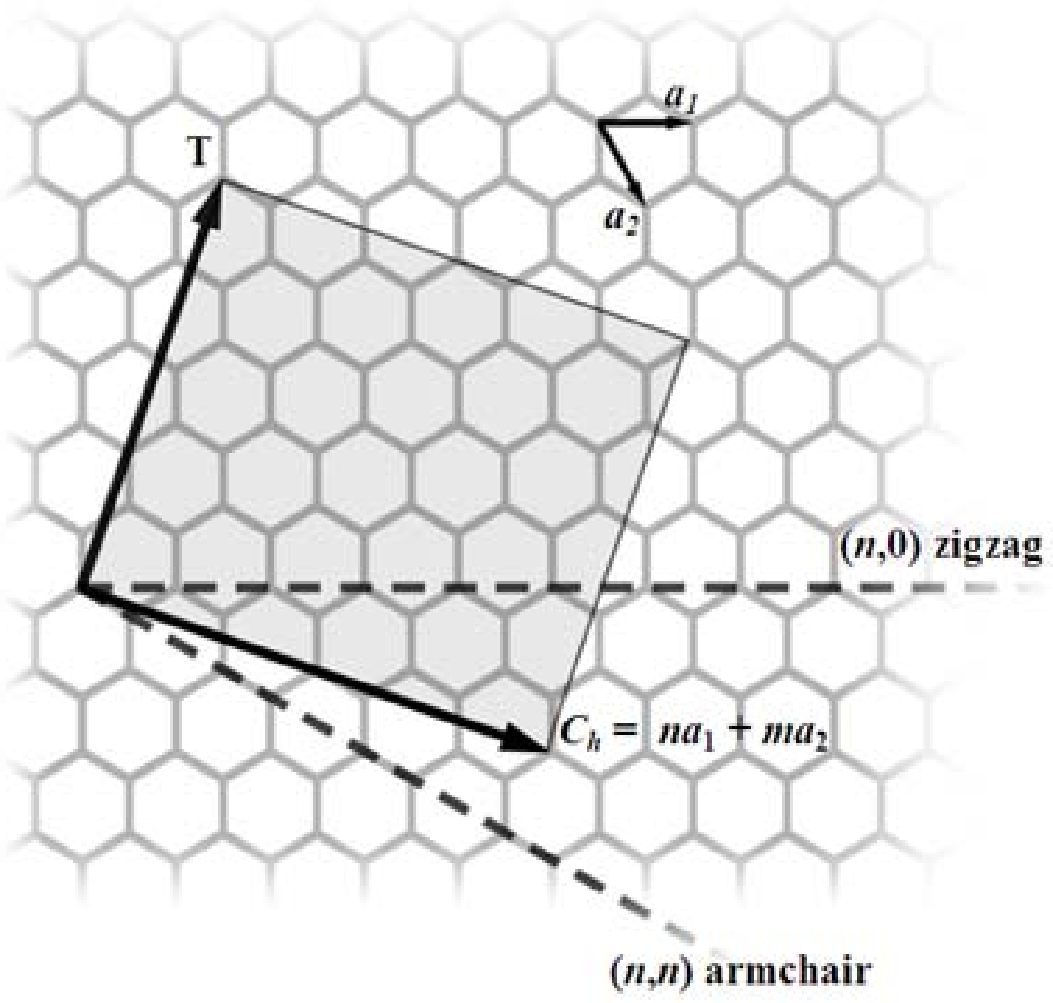

Figure 1.1: Integers n and m for Describing the Chirality of SWNT [13]

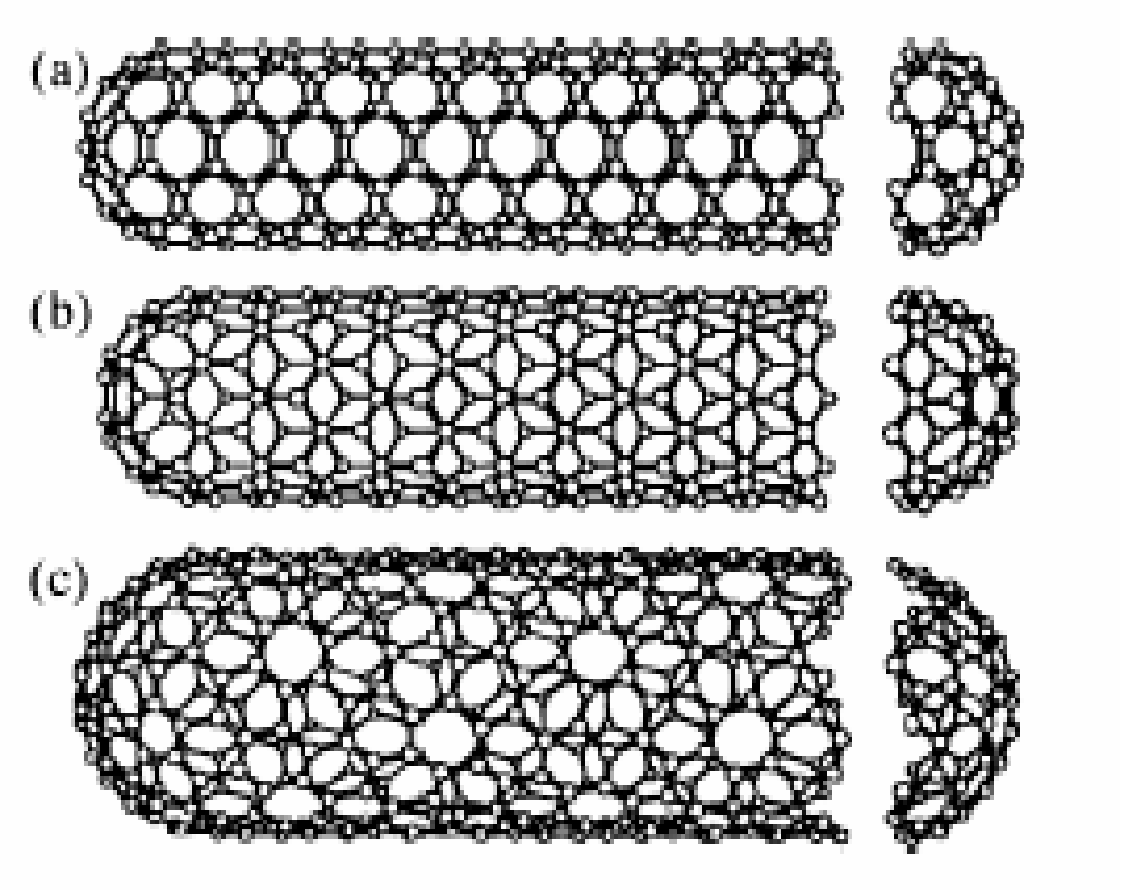

Figure 1.2: Different Chiralities of SWNTs (a) armchair, (b) zigzag, and (c) chiral [14]

Biological Applications of SWNTs

When introduced to biological systems, often SWNTs are able to translocate across the biological barriers such as membranes and tissues because of their hydrophobic surfaces. The relative higher surface areas of the SWNTs have been utilized to deliver therapeutically active molecules such as enzymes, peptides, DNA, RNA, as well as drug molecules [15, 16, 17, 18]. Besides, isolated SWNTs have their signature optical properties such as specific UV

absorbance and near infrared fluorescence, which enable the tracking of the nanoparticles inside biological systems. [19,20]

Pantarotto et al. determined that fluorescently labeled SWNTs covalently bound with bioactive peptides could penetrate cellular and nuclear membranes [16]. They also showed that both SWNTs and MWNTs can be covalently modified by pyrrolidine rings, with each bearing a free amino-terminal oligoethylene glycol moiety attached to the nitrogen atom. The presence of these functional groups led to a much increased solubility of the CNTs in aqueous solutions. Plasma DNA, encoded with marker gene (β-galactosidase; β-gal), was attached to positively charged ammonium functionalized CNTs via electrostatic interaction. Nuclear localization and translocation of CNTs through plasma cell membranes were observed with TEM. The uptake mechanism hereby was thought to be the binding of the cationic functional groups on the CNTs to the generally negatively charged cell membranes, which facilitated the spontaneous insertion of the CNTs across the cell membranes. Subsequent translocation and diffusion of the functionalised CNTs within the intracellular space could occur following these non-endocytotic processes. The rate of gene transfection was found to be dependent on the charge ratio of the ammonium groups on the SWNT surface to the phosphate groups of the DNA backbone. Gene expression efficiencies of 5-10 times higher than those without the presence of SWNTs were obtained. Gene expression also increased with incubation time of up to 3 h and decreased thereafter.

Our group first demonstrated the delivery of RNA polymer poly(rU) to MCF7 breast cancer cells using SWNTs as transporters [18]. Because of the hydrophobic interaction as well as the pi-stacking between the SWNT surfaces and the nitrogenous bases of the RNA, SWNTs were well solubilized by RNA in aqueous solution. After incubation with MCF7

cancer cells, we located fluorescently labeled SWNT-poly(rU) hybrids on cell membranes, in the cytoplasm, and in the nuclei of MCF7 cells utilizing the sectioning property of confocal fluorescence microscopy. We also performed radioisotope labeling, cell enumeration, and MTS assay which measured cellular metabolic activity through absorption. These studies provided information on the direct cellular uptake and the cytotoxicity of SWNTs. We postulated that the uptake of the SWNTs-poly(rU) was due to the amphipathic properties of both the cellular membranes and the SWNT-poly(rU) hybrids. The passive diffusion of membrane phospholipids and the hybrids, as well as the telophase of cell mitosis could also encase SWNTs. It was noted that both our cell growth and MTS studies showed no cytotoxicity in either MCF7 cells or d2C keratinocytes for SWNTs of concentrations up to 1 mg/mL.

In one of the most exciting developments thus far, Dai's group reported gene silencing with SWNT delivery [21]. The delivered siRNA was capable of silencing the gene encoding lamin A/C protein. Phospholipids (PL) were adsorbed onto SWNTs and the head groups of the PL were covalently linked to single-chained poly(ethylene glycol) (PEG) with terminal amine or maleimide groups (PL-PEG-NH2 or PL-PEG-maleimide). The PL-PEG bound to SWNTs via van der Waals and hydrophobic interactions between the fatty alkyl chains of the PL and the sidewalls of the SWNTs. Although double-chained PL molecules alone did not solubilize SWNTs, the presence of the PEG greatly increased the hydrophilic moiety of the PL-PEG-SWNT complexes, thus rendering SWNTs water soluble. In the silencing assay, PL-PEI functionalized SWNTs transported siRNA into HeLa cells, and the disulfide bonds linking the siRNA and the phospholipid-PEI were cleaved off by the enzymes in acidic lysosomes. The translocation of SWNT complexes across cell membranes

was hypothesized to result from endocytosis and no adverse effect on cell viability or proliferation was found in the presence of SWNTs. The silencing potency using siRNA was a two-fold increase as compared with commercial lipofectamine delivery, and this increased efficiency was attributed to the high surface area and high intracellular transporting ability of SWNTs, as well as the high degree of endosome/lysosome escape after the cleavage of the disulfide bond.

Kam et al. explored protein delivery with SWNTs [22]. Streptavidin (SA), protein A (SpA), BSA, and cytochrome c (cytc) proteins were fluorescently labeled and bound to the sidewalls of SWNTs via adsorption. The translocation of these proteins in mammalian cell lines, including HeLa, NIH-3T3 fibroblast, HL60, and Jurkats cells, were observed with confocal fluorescence microscopy. Lowering temperature to 4°C yielded little uptake, indicating that endocytosis was responsible for the uptake of the nanomaterials at room temperature. Cellular uptake of large proteins (MW > 80 kDa) was poor, while the intracellular transport of proteins by SWNTs appeared to be general for small- and medium-sized proteins. SWNT-protein conjugates, once internalized within the cells, were co-localized with the red endocytosis endosome marker FM 4-64; suggesting the confinement of the conjugates in endosomal lipid vesicles. NIH-3T3 cells are known to undergo cytc-induced apoptosis which can be analyzed using FITC-labelled Annexin V, an efficient marker for early stage apoptosis. Indeed, significantly higher percentages of apoptosed cells were observed for NIH-3T3 cells incubated with cytc-SWNT conjugates than with cytc alone. To investigate the effect of endosomal release on the efficiency of apoptosis induction by cytc, cells were incubated with cytc-SWNT in the presence and absence of chloroquine, a membrane-permeable base that can localize inside endosomes and cause increases in pH.

Higher degrees of apoptosis were observed for cells treated with cytc-SWNT in the presence of chloroquine. This higher degree of apoptosis is due to the more efficient endosomal releasing of proteins, suggesting that the cytoc transported by SWNTs remained biologically active for apoptosis induction. However, it is unclear if the functionality of cytoc was retained after detached from the SWNTs, or if it remained active even when proteins were still attached to the SWNTs.

SWNTs show distinct photophysical properties, such as fluorescence, which are only available at the single particle level [20, 23]. These properties may be used for sensing DNA polymorphism, imaging nanoparticle translocation, or for developing new cancer therapeutics. Kam et al. demonstrated a scheme for the selective destruction of cancer cells [24]. In this scheme, SWNTs were conjugated with various phospholipids (PL), a polyethylene glycol (PEG) moiety, and a terminal folic acid (FA) group that provided specificity for folic acid-starved HeLa cells. SWNTs conjugated with the folate moiety were internalized by the cells and were consequently irradiated with a near-infrared laser to induce the first and second van Hove optical transitions of the isolated tubes. The optical stimulations of SWNTs, transferred to molecular vibration energies and heat within minutes, eventually destroyed folate-starved cancer cells. Healthy cells without folate deprivation showed little SWNTs translocation and remained viable due to the biocompatibility of the near-infrared wavelength.

Heller et al. observed a red shift of the SWNT band-gap fluorescence when an encapsulating 30-nucleotide oligomer was exposed to counter-ions that screened the charged DNA backbone [25]. The transition was thermodynamically identical for DNA on and off the nanotube, except that the propagation length of the former was shorter by five-sixths.

Based on the fluorescence profiles of SWNTs, Heller et al. characterized the B to Z conformational transition of DNA on the nanotubes in the presence of divalent chloride counter-ions. This remarkable transducing capacity of SWNTs can, in principle, be used for ion detection in media already possessing a strong ionic background.

Bianco's group took a survey on different type of functionalized SWNT. They found cellular uptake of functionalized SWNT is independent of functional group and cell type [26]. The transportation of functionalized SWNT was observed a few hours following initial contact with the cells, even under endocytosis-inhibiting conditions. The mechanisms are most likely to be energy-independent.

Structure of Fullerenes

As introduced before, fullerenes are the number four allotrope of carbon. They share similar structure with graphite to some extent. Fullerenes are composed of a sheet of linked hexagonal rings, but they also contain pentagonal rings that prevent the sheet from being planar. C_{60} and C_{70} are the most abundant fullerene molecules. Other fullerenes that have been produced in macroscopic amounts have 76, 84, 90, and 96 carbon atoms. Much larger fullerenes have been found, which contain 180, 190, 240, and 540 carbon atoms [27, 28].

C_{60}, discovered in 1985, is the first and archetypal member of the fullerene family [29]. In C_{60}, sixty carbon atoms are arranged over the surface of a hollow cage. Each atom is trigonally linked to its three neighboring atoms by bonds that delineate a polyhedral network, consisting of 12 pentagons and 20 hexagons. All 60 atoms in a C_{60} molecule are equivalent and lie on the surface of a sphere distributed with the symmetry of a truncated icosahedrons

[30]. The 12 pentagons are isolated and interspersed symmetrically among 20 linked hexagons.

C_{70}, the other most studied fullerene molecule besides C_{60}, display a 'rugby ball' structure with electron diffraction, with a slight pinching of the waist [31]. With 12 pentagons and 25 hexagons of carbon rings, the elongated structure reduces the symmetry of C_{70} than C_{60}, consequently endows it with different photo properties such as absorbance and fluorescence.

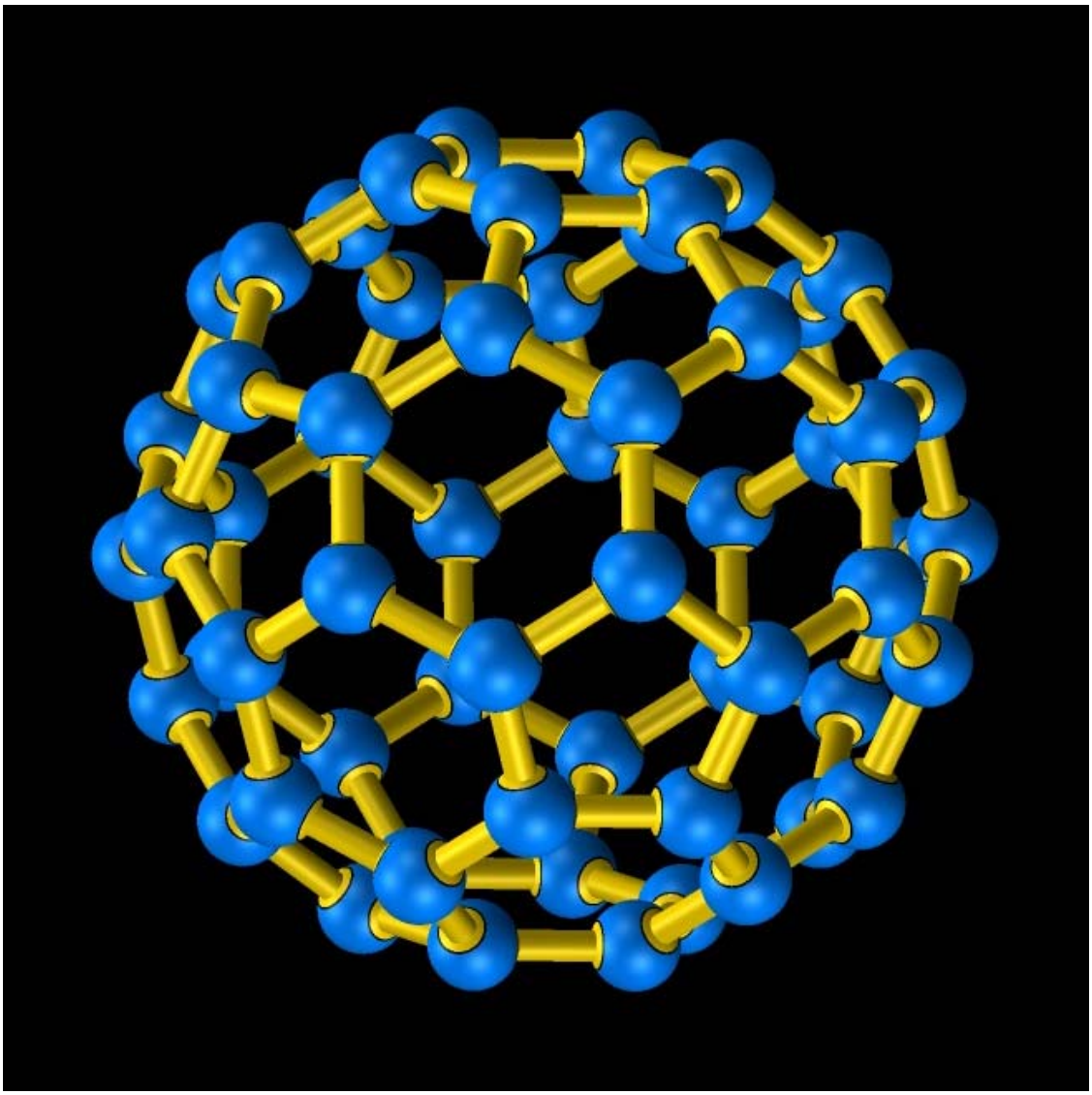

Figure 1.3: Structure of C_{60} [32]

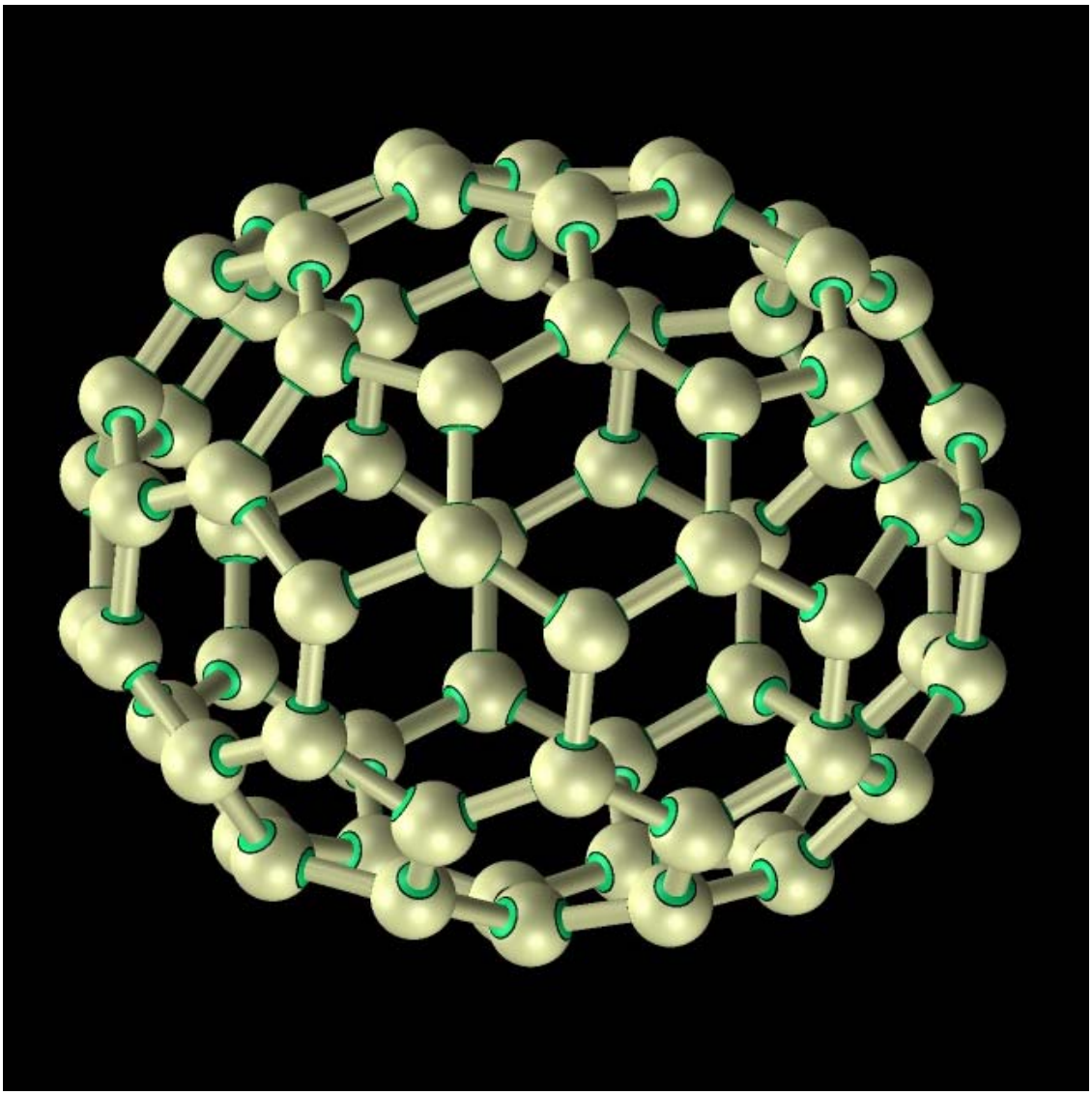

Figure 1.4: Structure of C_{70} [33]

Applications of Fullerenes

Cage-like fullerene molecules represent another class of carbon-based nanomaterials with unique structural, mechanical, and electronic properties. Unlike the SWNTs, fullerenes have even smaller structures in the shape of buckyball or rugby ball with the diameter around 1 nm. When interacting with biological systems, fullerenes have been found applications as neuroprotective agents [34], HIV-1 protease inhibitors [35, 36], antioxidants [37], X-ray contrast enhancers [38], and drug delivery transporters [39]. Due to their mutual van der Waals interaction, fullerenes readily accumulate and their aggregates can facilitate electron transfer across cell membranes, a phenomenon which could impact on photosynthesis and biomedicine [40, 41].

Using model building technique, Kenyon's group examined the ability of C_{60} derivatives to interact with the active site of HIV-1 protease [35]. The result suggests that C_{60} derivatives will fit snugly in the active site, thereby removing 298 Å2 of primarily nonpolar surface from solvent exposure and driving ligand-protein association. The active site of this enzyme can be roughly described as an open-ended cylinder which is lined almost exclusively by hydrophobic amino acids (Figure 1.5). Notable exceptions to this hydrophobic trend are the two catalytic aspartic acids (Asp 25, Asp 125) which catalyze the attack of water on the scissile peptide bond of the substrate. Since a C_{60} molecule has approximately the same radius as the cylinder that describes the active site of the HIVP and since the derivatives of C_{60} is primarily hydrophobic, an opportunity therefore exists for a strong hydrophobic interaction between the C_{60} derivative and active site surfaces. This interaction could make C_{60} derivatives inhibitors of the HIVP.

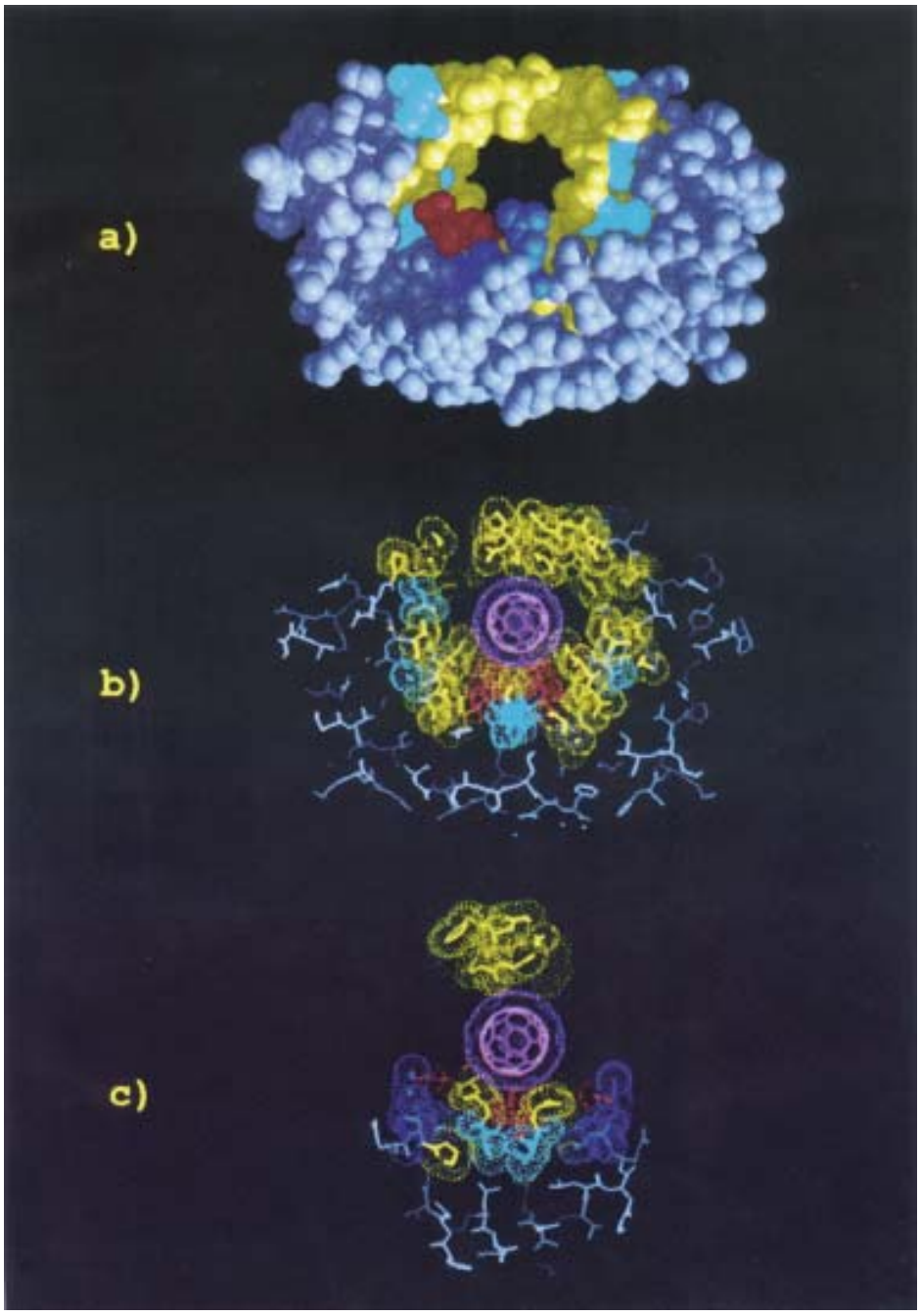

Figure 1.5: Simulation Structure of HIV-1 Protease and C_{60}. (a) "Front" view of the HIV-1 protease. (b) Same view as (a) with the top scoring C_{60} orientation shown. The C_{60} is colored magenta, and the *van der Waals* surface of the active site and ligand are shown. (c) Same complex as (b) seen at a 90° cross section [35].

Mauzerall's group found out that C_{70} aggregates in the lipid bilayer created an electronic channel and provided fast negative charge transport [40, 41]. Electron transport across lipid membranes is a fundamental property of living systems and is exemplified in photosynthesis. Since the photophysics of fullerene molecules resembles that of porphyrins and the fullerenes have low reduction potentials, they are expected to have interesting charge-transfer chemistry in both the ground state and the excited states. C_{60} and C_{70} embedded within a lipid bilayer can act as efficient electron acceptors from electron donors at the interface. Furthermore, fullerenes can also efficiently transport negative charge completely across the membrane. Mauzerall et al. used photovoltage and photocurrent measurements on the systems and presented evidences that the charge transfer is most likely by electronic conduction mediated by fullerene aggregates.

Larroque et al. demonstrated that a fullerene derivative could cross the cellular membranes and it localizes preferentially in the mitochondria [42]. They showed by fluorescence microscopy that fullerene derivative $C_{61}(CO_2H)_2$ was able to cross the cell membrane. Using radioactive labeling they also showed that the fullerene preferentially bound to mitochondria. The generation of oxygen-free radicals in cells came from the leakage of electrons from the mitochondrial electron transport chain. This observation suggested the use of fullerenes to mediate the delivery of drugs across cell membranes and tissues.

Wilson's group synthesized and characterized a new water-soluble C_{60} derivative designed to covalently attach to proteins such as ZME-018 as an initial step toward targeted fullerene immunotherapy [39]. A single-drug chemotherapeutic agent such as a recently reported C_{60}–paclitaxel conjugate could be employed for FIT, but the real advantage of FIT

over other targeted therapeutic agents is the potential for the attachment of multiple (and possibly different) drugs to the C_{60} scaffold in order to create targeted, single-dose "drug cocktails".

Fluorescence

Fluorescence is a process distinct from incandescence (i. e. emission of light due to high temperatures). Heating is generally detrimental to the process of fluorescence, and most substances, when fluorescing, produce very little heat. For this reason fluorescence has commonly been referred to as "cold light".

In the standard conceptual model of molecules electrons occupy distinct orbitals and thus energy levels. This is a simple view of molecules, but it does serve to outline the general process of fluorescence. A common result of directing light on a molecule that absorbs rather than transmits is that one or more of the electrons of the molecule are "kicked" into a higher energy state. (Figure 1.6) All these excited electronic states are unstable, and sooner or later the electrons will lose their excess energy and fall back to lower energy states. This excess energy can be dissipated in several ways, the most common being simply to increase atomic vibrations within the molecule. But some molecules are capable of converting some of the energy to light. Both absorption and radiation (emission) spectra are unique characteristics of a particular molecule (structure) during the fluorescence process. Light is absorbed by molecules in about 10-15 seconds which causes electrons to become excited to a higher electronic state. The electrons remain in the excited state for about 8-10 seconds, then, assuming all of the excess energy is not lost by collisions with other molecules, the electron returns to the ground state. Energy is emitted during the electrons' return to their

ground state. Emitted light always has a longer wavelength than the absorbed light due to limited energy loss by the molecule prior to emission.

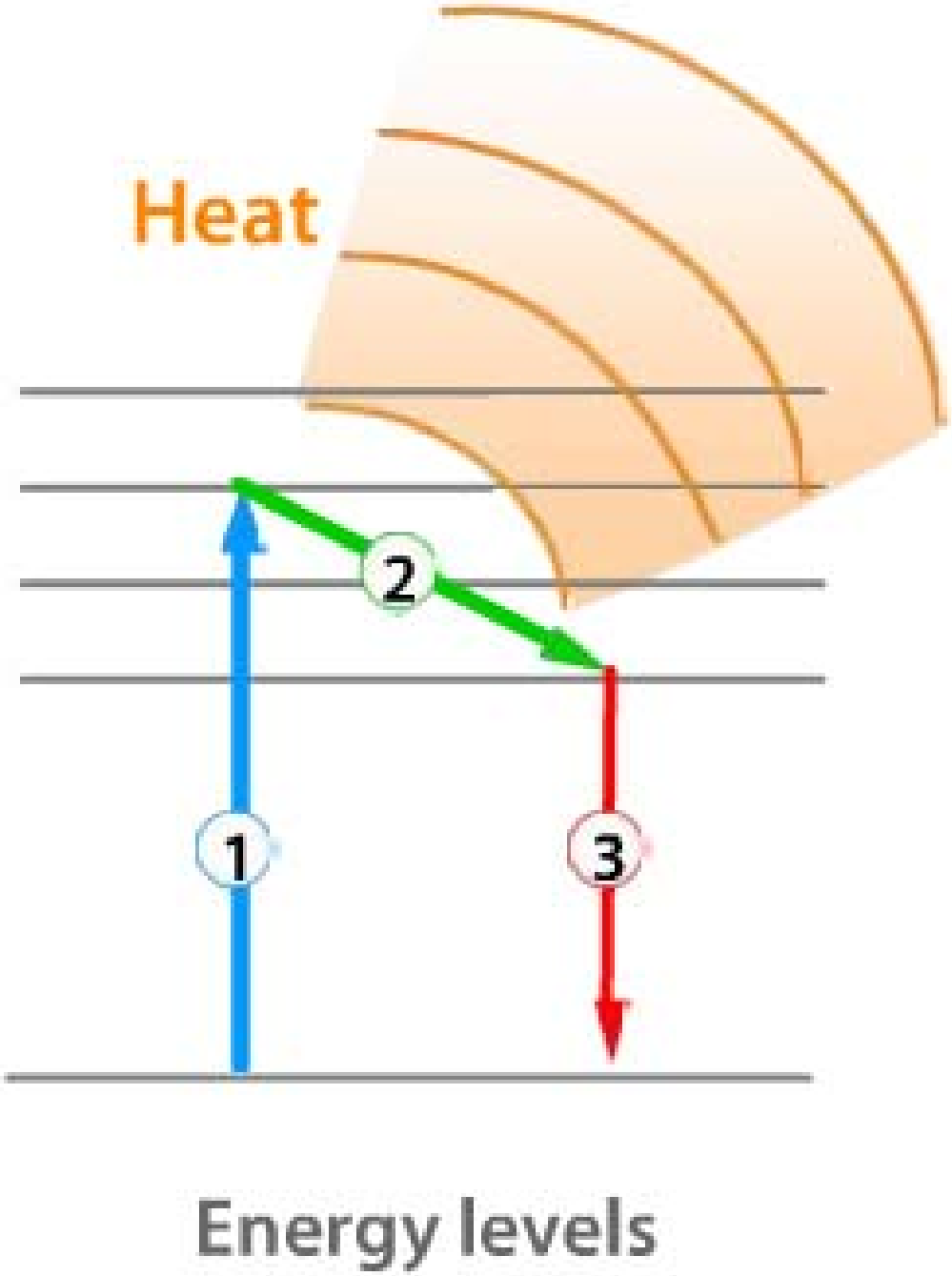

Figure 1.6: Mechanism of Fluorescence [43]

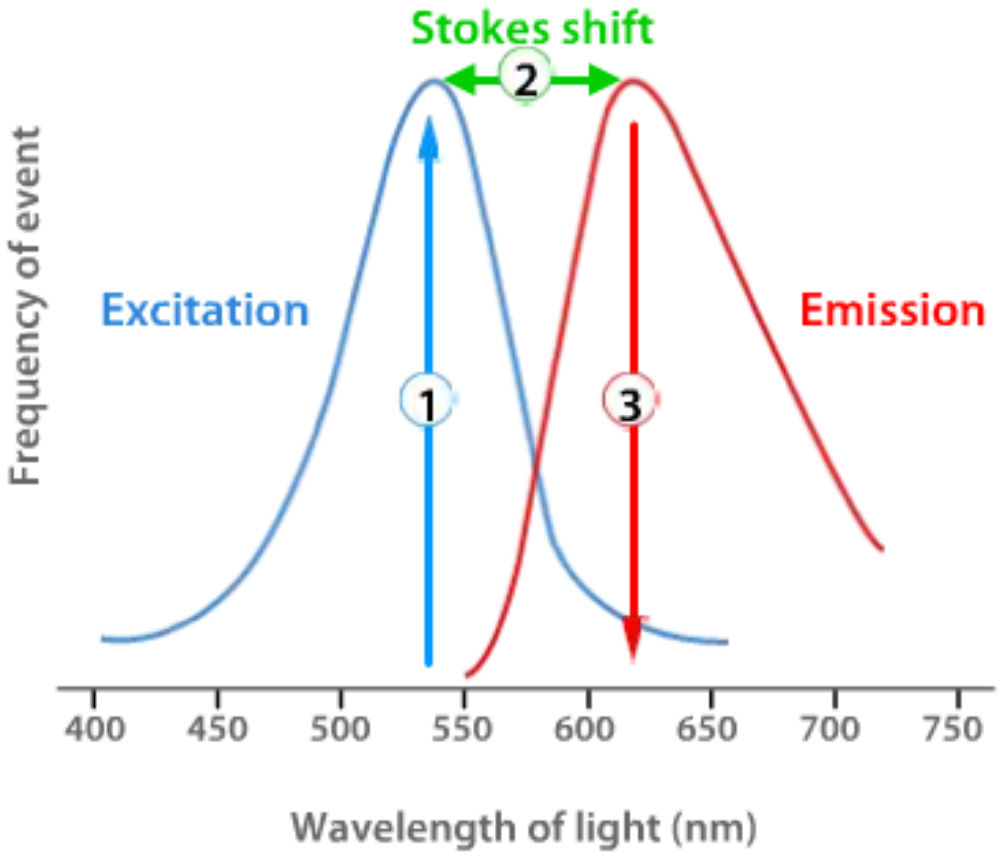

Figure 1.7: Fluorescence Excitation and Emission [43]

FRET

Fluorescence resonance energy transfer (FRET) occurs as a result of the energy transfer between two chromophores. A fluorescent donor is excited at a specific wavelength. By a long-range dipole-dipole coupling mechanism, this excited state is then nonradiatively transferred to a second molecule, the acceptor. The donor returns to the electronic ground state and the acceptor emits its fluorescence concomitantly. FRET is a highly distance-

dependent interaction between the electronic excited states of the two dye molecules. The efficiency of FRET is described by the inverse sixth power of the intermolecular separation, making it useful over distances comparable with the dimensions of biological macromolecules. Thus, FRET is an important technique for investigating a variety of biological phenomena that produce changes in molecular proximity [44].

The primary conditions for FRET are as followed:

a. Donor and acceptor molecules must be in close proximity (typically 10 ~ 100 Å).

b. The absorption spectrum of the acceptor must overlap the fluorescence emission spectrum of the donor (Figure 1.8).

c. Donor and acceptor transition dipole orientations must be approximately parallel.

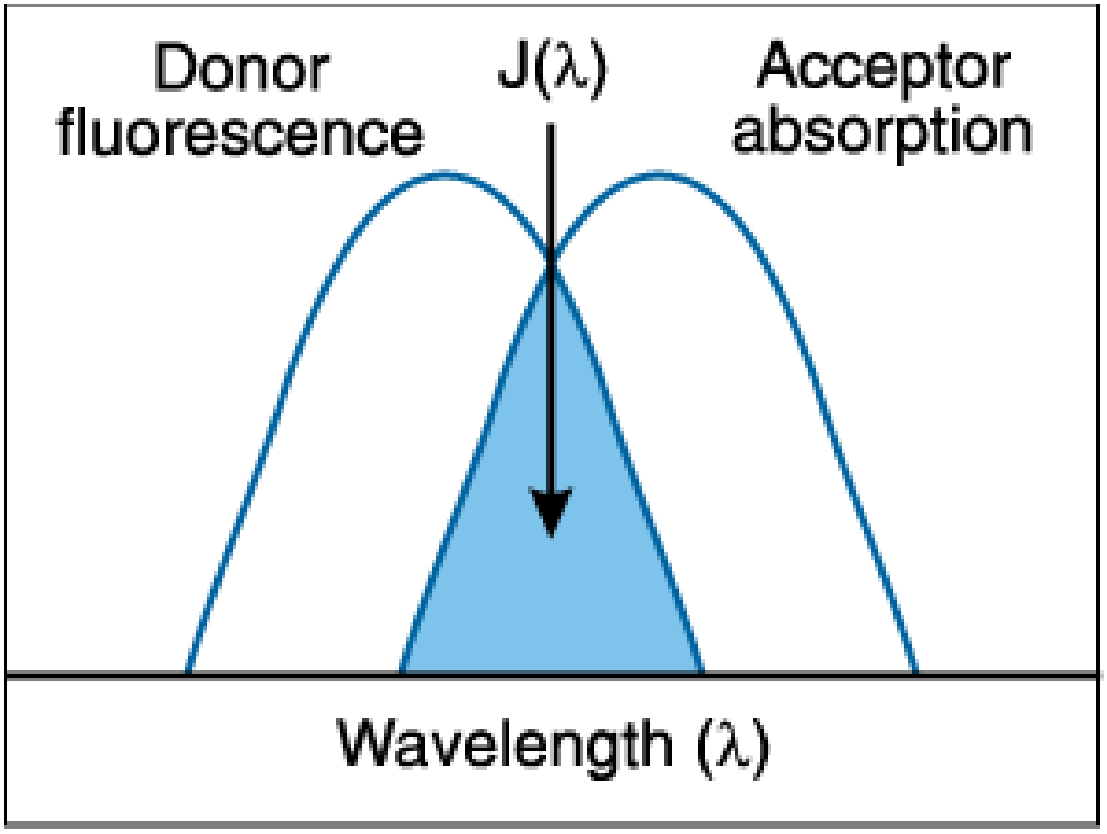

Figure 1.8: Schematic Representation of the FRET Spectral Overlap Integral [45]

Nanotoxicity

Nanoparticles, billionth of a meter in dimensions, produced by nature or nanotechnology, have unusual properties not found in the bulk materials, which are exploited in numerous applications such as biosensing, electronics, photovoltaics, diagnostics, and drug delivery. However, recent years have witnessed a range of potential health hazards of nanomaterials, which calls for research into the area of nanotoxicity. Because of the small sizes and large surface areas of nanomaterials, even when they are made

of inert elements like gold, may become very active at a nanometer scale. Nanotoxicological studies are intended to determine whether and to what extent these may pose a threat to the environment and to human health.

Researchers at the University of Texas found that carbon nanotubes squirted into the trachea of mice caused serious inflammation in the lungs and granulomas, and five of the nine mice treated with the higher dose died [46]. In a similar experiment carried out at the National Institute of Occupational Safety and Health in Morgantown, West Virginia, researchers not only found granulomas in the lungs, but also damage to mitochondrial DNA in the heart and the aortic artery, and substantial oxidative damage, both foreshadowing atherosclerosis [47].

In yet another similar experiment in Tottori University, Japan, researchers showed that within a minute of contacting the mice's tiniest airways, carbon nanotubes began to burrow through gaps between the surface lining cells and into the blood capillaries, where the negatively charged nanoparticles latched onto the normally positively charged red blood cells surface, thereby potentially causing the red blood cells to clump and the blood to clot [48].

Researchers at the University of Rochester, New York, reported an increased susceptibility to clotting in rabbits that had inhaled buckyballs [49]. Buckyballs presented in water at 0.5 ppm were taken up by largemouth bass, which suffered severe brain damage 48 h later, the extent of damage being 17 times greater than that seen in controls. Nanoparticles in the lungs were translocated into the circulatory system and throughout the body, and accumulated in the liver, spleen, and bone marrow [49]. When inhaled through the nose and

air passages, nanoparticles were translocated to the brain through the olfactory nerves, and accumulated in the brain [50].

All above studies show the potential detrimental effects of nanomaterials to the environment as well as the human health. Since none of these studies used consistent protocols for nanomaterials preparation and solubilization, there remains much work to be done on the synthesis of nanomaterials as well as understanding the consequences of nanomaterilas interacting with biological systems or discharged into the environment.

CHAPTER TWO

BINDING OF LPC-SWNT FOR SOLUBILITY AND BIOAVAILABILITY

Single-walled carbon nanotubes (SWNTs) offer numerous excellent properties which can be applied into different fields. However, because of their inherent hydrophobicity, applications involving SWNTs in the liquid phase must first overcome their insolubility. Previous studies have shown two major routes to solubilize SWNTs. One is chemical method which modifies the surfaces of SWNTs by covalently bonding with certain hydrophilic functional groups. The other physical method shields the hydrophobic surfaces of SWNTs via hydrophobic interaction and/or pi-stacking with amphiphiles. The significant advantage of the physical method over the chemical method is that the former preserves the properties of SWNTs.

In this chapter, I will present our invented physical method for solubilizing SWNTs using amphiphilic lysophospholipids (LPL). The superior water solubility of LPL-SWNT enables the translocation of SWNTs across cell membranes as well as our investigation of the environmental impact of SWNTs.

Literatures on Binding Models of SWNT-amphiphilie Supremolecular Complex

Previous studies have shown that amphiphilies such as lipids afford a significant solubility for SWNTs in aqueous solution. In the current literature there are three models detailing the structures of such interaction: cylindrical micelles, randomly absorption, and hemimicelles [51, 52, 53]. Matarredona et al. examined the dispersion of SWNTs in the surfactant sodium dodecylbenzenesulfonate (NaDDBS) using CoMoCAT synthesis. They

noted that the electrical charge of the SWNT surface varied with the pH of the surrounding media, but that Coulombic forces between the anionic NaDDBS and the SWNT were overcome by the hydrophobic interaction between the surfactant tail and the nanotube sidewall. Only at pH values far from the point of zero charge did Coulombic forces prevail. In other words, the hydrophobic forces between the surfactant tail and the nanotube surface mainly determined their self assembly. Yurekli et al. described a different scenario of carbon nanotube-amphiphile binding based on their SANS study of SWNT dispersion with SDS. They found no preferential arrangements of the head and tail of the surfactants responsible for the stabilization of the dispersion. The SANS data were fit with Percus-Yevick closure for hard spheres and no agreement with the cylindrical micelle model was reached for SDS of either below or above the Critical Micelle Concentration (CMC, 0.2 wt% for SDS). Richard et al. suggested the possibility of hemimicellar binding based on their TEM study of SDS and synthetic lipids interacting with both single-walled and multi-walled carbon nanotubes. They noted, however, that only SDS at above the CMC could form superstructures of rolled-up half cylinders on the nanotube surface. Depending on the symmetry and the diameter of the carbon nanotube, rings, helices, or double helices were also observed with TEM and cryo-TEM. However, since cryo-TEM involves solvent sublimation, it remains unclear to what degree these ordered structures in a vacuum truly manifest their liquid phase.

It is noted that all the three models above are concerning the binding of small amphiphilic molecules onto nanotubes. In the case of relative large molecules such as DNA and RNA, helical wrapping is another proposed binding mechanism. The molecular-level picture of helical wrapping was proposed by O' Connell et al. when describing the binding of

amphiphilic polymers (PolyVinyl Pyrrolidone (PVP) and PolyStyrene Sulfonate (PSS)) onto SWNTs [54]. Since a single tight coil would necessarily introduce significant bond-angle strain in the polymer backbone, enough to offset the thermodynamic drive for wrapping, the authors postulated that multi-helical wrapping could be responsible for the dispersion of SWNTs in polymer solutions. This is because multi-helical wrapping would allow high-surface area coverage with low-backbone strain, and multiple strands of the polymer would coil around the SWNT close to its nascent backbone curvature. Using Molecular Dynamics (MD) Zheng et al. illustrated the binding of ssDNA on an SWNT surface as helical wrapping [55]. In addition to interactions between the nitrogenous bases of the ssDNA and the hydrophobic tube surface, the assembly was believed to be further stabilized by the stacking between the bases of the ssDNA and the p-electrons of the carbon atoms. Consequently, the SWNT solubility was afforded by the negatively charged sugar-phosphate backbone of the ssDNA. Thermodynamics calculations by the authors predicted that the binding enthalpy was comparable with the energy required for individual tubes to bundle, and dominated the free energy of binding. In a recent study by Dieckmann et al., the interaction of SWNTs and peptides was modeled using the package Insight- II, subjected to energy minimization using Discover and Consistent Valence Force Field [56]. The binding of individual amino acids of the peptides with the sp2-hybridized carbon atoms of the SWNT was monitored, where parallel helical wrapping on the SWNT was found feasible for up to 6 a-helices without terminal charges.

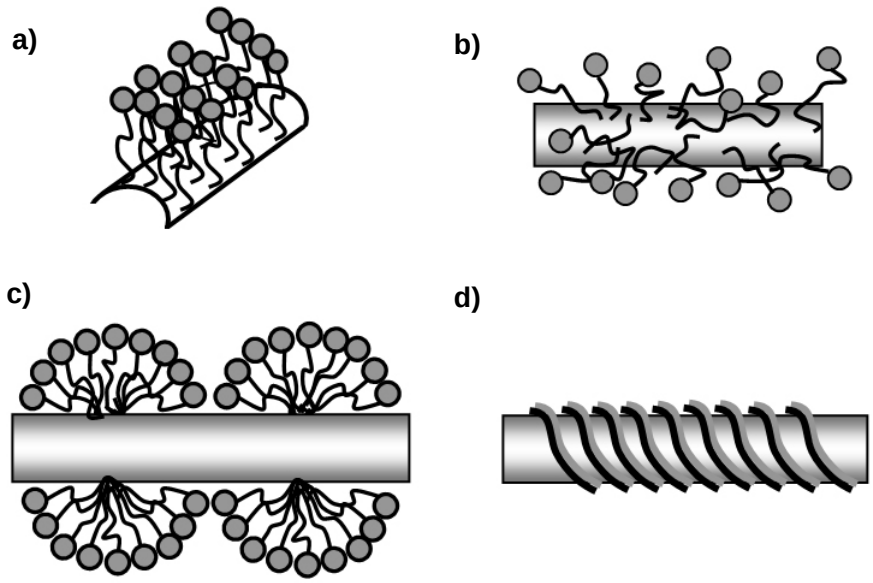

Fig 2.1: Four Representative Models of Supramolecular Amphiphile-nanotube Complex

Experiments for Solubilizing SWNTs Using Different Amphiphilies

Molecular structure dependence

To render SWNTs soluble in aqueous solution, amphiphiles lysophosphotidylcholine (LPC), sodium dodecyl sulfate (SDS) and dihydroxy-L-phenylalanine (DOPA) (Figure 2.2) were employed to obtain different levels of solubility of SWNTs. SWNTs and LPC, SDS and DOPA were mixed at the weight ratio of 1:5, and put into tubes which were filled with distilled water. Probe sonication was conducted for 30 min (VC 130 PB, Sonics & Materials) at 7 W at room temperature. The solution was centrifuged for 3 min at 7.5*103 RPM/min, and the supernatant was taken out for further measurement.

The properties (hydrophobicity, steric structure) of these three amphiphiles affected the concentrations of SWNTs in solutions. Centrifuged solution of SWNT-LPC, SWNT-

SDS and SWNT-DOPA were put into cuvettes and their absorbance measured at 360 nm using a spectrophotometer (Shimadzu, UV 1601). As shown in Figure 2.3, LPC is the most efficient molecule to solubilize SWNT, approximately 3 time better than SDS and 5 times better than DOPA. These differences might be because LPC has a bulkier head group for interfacing with water and a longer acyl chain for binding to SWNTs compared to SDS (Figure 2.2). On the other hand, DOPA only has one benzene ring which can form pi-stacking with SWNT, which offers the lowest solubility. All supramolecular complexes show promising stability under room temperature (25 ºC) over certain period (6 days).

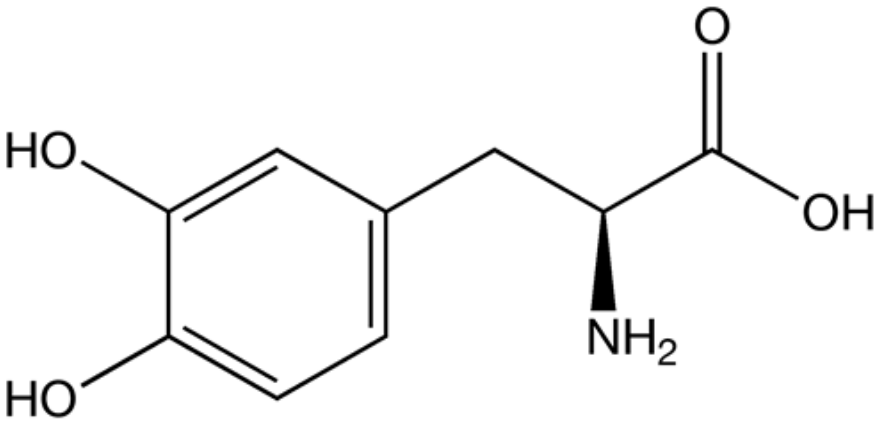

DOPA

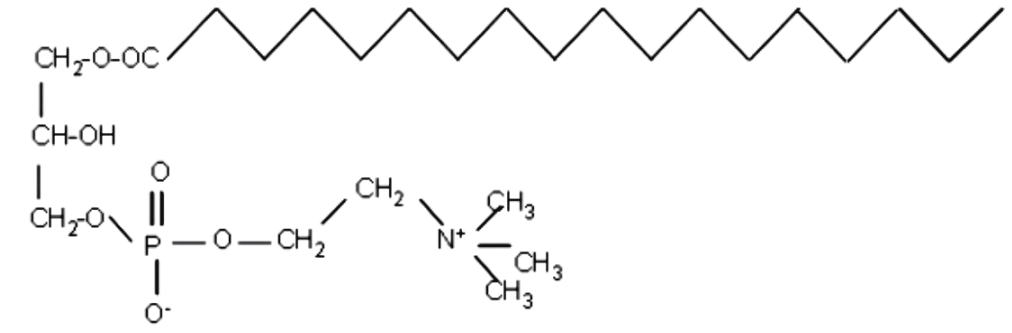

LPC 18:0

SDS

Figure 2.2: Structures of DOPA, LPC and SDS

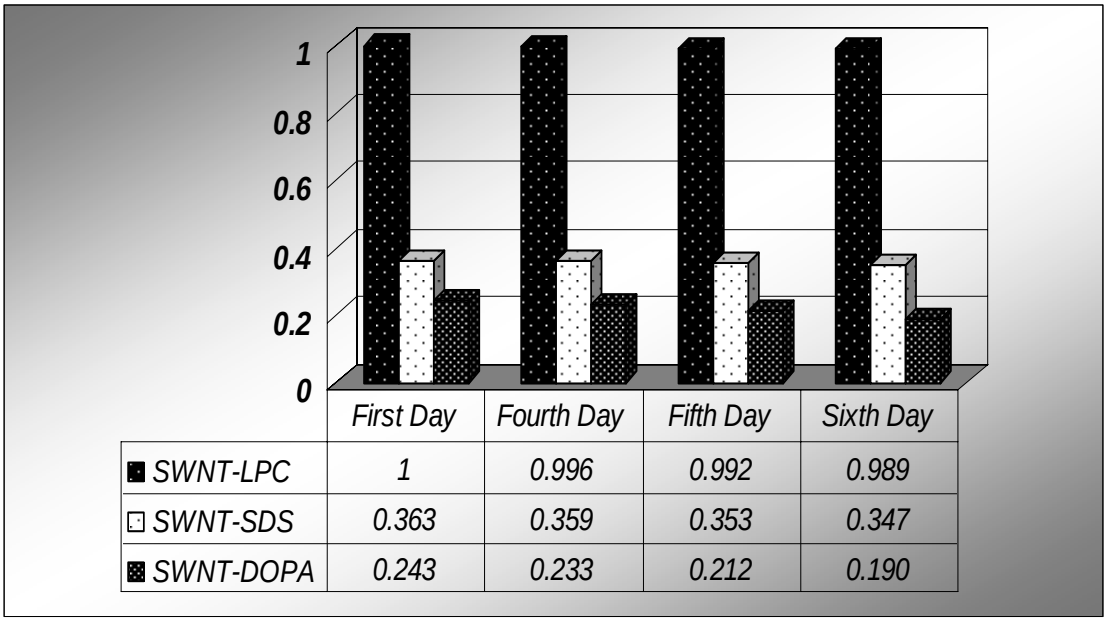

Figure 2.3: Stability of SWNT-LPC, SWNT-SDS, and SWNT-DOPA Over Time

Ionic Strength, Temperature and pH Dependence

NaCl and CaCl2 of 20 mM were mixed with SWNT solutions respectively. The induced SWNT concentration changes were evaluated by absorbance measurements. Figure 2.4 shows the ionic dependences of SWNT-LPC, SWNT-SDS and SWNT-DOPA complexes in water. After adding salts, all solutions underwent concentration decreases. In particular, the absorbance of SWNT-LPC dropped by 18% and 20.8% after adding sodium and calcium. Similar decreases occurred for the other two solutions. Among which, the decrease due to the addition of calcium was much more pronounced than sodium. The possible explanation is because each calcium ion bridged between the head groups of two LPC or SDS molecules, thus reducing the stability of their supramolecular complex

structures with SWNTs. In the case of DOPA, calcium ions reacted with DOPA and formed white powder like substance, which dissociated the SWNT-DOPA complexes.

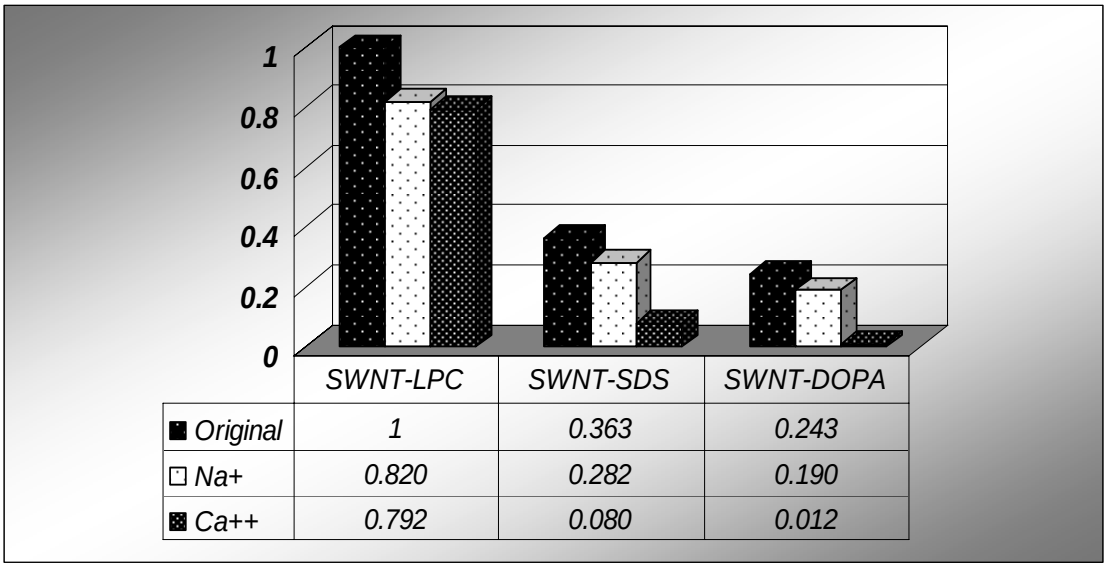

Figure 2.4: Absorbance of SWNT-LPC, SWNT-SDS, and SWNT-DOPA in the Presence of Na^{+} and Ca^{2+} Ions

The temperature dependence of SWNT-LPC was measured against a blank at 360 nm using a spectrophotometer (Shimadzu, UV-1601). The temperature was adjusted between 7 to 95°C using a temperature control module. The absorbance readings were obtained in two consecutive measurements by first heating up and then cooling down the water bath. These two measurements yielded less than a 2% discrepancy of absorbance for corresponding temperature readings. The result was shown in Figure 2.5. The temperature dependence of the SWNT-LPC assembly suggests that SWNTs and LPC comprised single

entities as a whole, rather than dynamic equilibria of supramolecular associations in solution. This finding is important for the design and applications of SWNT-lipid assembly.

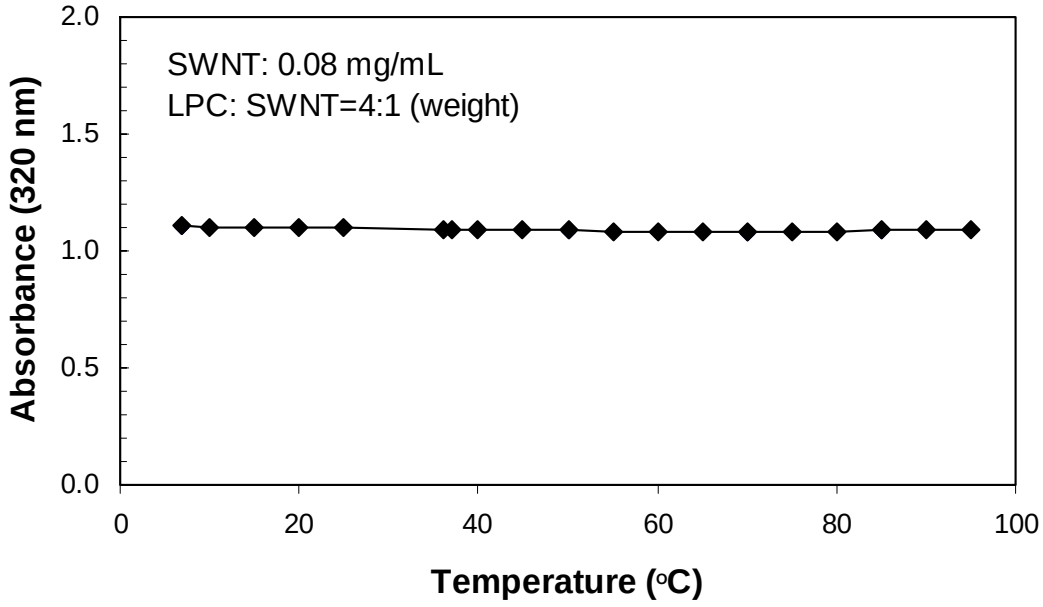

Figure 2.5: Temperature Dependence of SWNT-LPC Assembly in Water Solution.

Similarly, the pH dependence was measured against a blank at 360 nm using the same device for SWNT-LPC solubilized in Fluka buffer solutions (pH 2.5 and 4: 20 mM sodium citrate; pH 7 and 8: 20 mM sodium phosphate; and pH 9: 20 mM sodium tetraborate). These pH values were used to simulate the acidic to basic chemical and biological environments. This change of absorbance is due to the fact that a lower solvent pH yields a high proton concentration which could form more hydrogen bonds with the

negative moieties of the LPC head groups. Now that the zwitterionic LPC becomes net positively charged, the energy barrier is raised for the lipids to pack tightly against the SWNT surface.

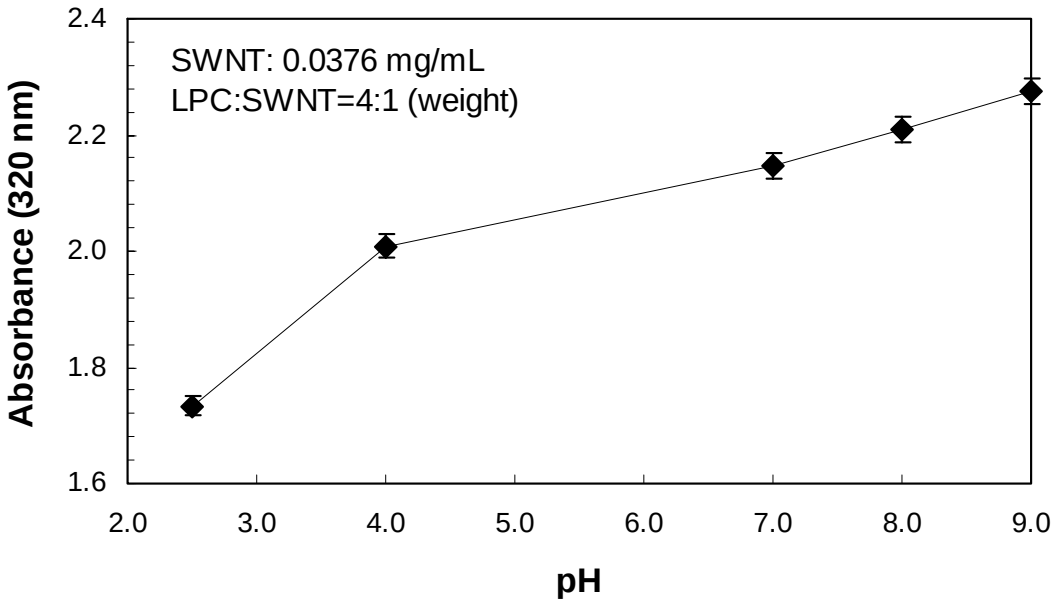

Figure 2.6: pH Dependence of SWNT-LPC Assembly in Fluka Solutions

Modeling

TEM imaging does not offer exact information on how individual lipids are arranged within the envelop of a striation, yet this information is key to resolving the debate on the nanotube-lipid assembly. It has become apparent that neither TEM nor absorbance-based methods can resolve the binding dynamics of SWNT-amphiphile with adequate temporal and/or spatial resolution. MD simulations are advantageous in those regards. Figure 2.7

displays the time evolution of lipid LPC 18:0 coated on an SWNT of 1.4 nm in diameter. Contrary to the literature, these illustrations show a tendency of lipids to orientate primarily along the SWNT axis. The exposure of hydrophilic lipid head groups to the water (not shown) displays a topology startlingly agreeable to that observed in the TEM studies, yet the arrangement of individual lipids distinctly departs from that in the hemimicellar model.

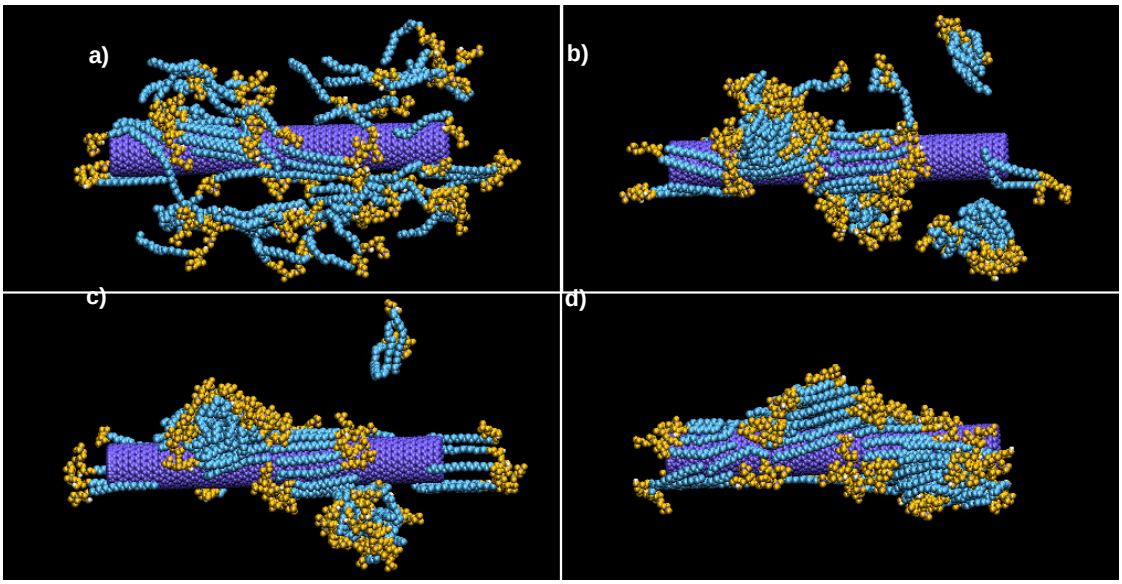

Figure 2.7: MD Simulations of the Self Assembly of LPC onto an SWNT. (1.4 nm in diameter and 11.8 nm in length). (a-d) The simulation system configurations at 0.2, 1.6, 6.4, and 17.9 ns, respectively. The lipid heads and tails are illustrated in gold and blue and the SWNT is in purple. Striations of lipids (~4.5 nm) are evident in panel d.

FRET Detection of SWNT Translocation

Following the demonstration of solubilizing SWNTs using lysophospholipids, rhodamine-labeled Lysophosphoethanolamine (LPE) was introduced to solubilize SWNTs. The supramolecular assembly of Rd-LPE-SWNT allowed us to track SWNTs inside cells

with the aid of rhodamine fluorescence. MCF7 breast cancer cells were cultured for the translocation experiment.

Solubilizing SWNT using Rd-LPE

To obtain LPE, one fatty acyl chain of lipid 1,2-Dipalmitoyl-sn-Glycero-3-Phosphoethanolamine-N-(Lissamine Rhodamine B Sulfonyl), (Rd-PE) (structure see Figure 2.8) was cleaved using enzyme phospholipase A2, which hydrolyzed the acyl group attached to the SN2 carbon of the Rd-PE. The best digestion was obtained with 30 μL of 0.1 M $CaCl_2$, 90 μL of 1 M NaCl, 3 μL of 1.5 M Tris buffer (pH 8.8), 300 μL of water, and 1.5 mg of Rd-PE. This mixture was sonicated for 10 min before the addition of 200 mL of a phospholipase A2 solution consisting of 1 mg phospholipase A2 in 1 mL of 0.15 M Tris buffer. Once combined, the digestion was allowed to run for 24 h in darkness on a shaker. At the conclusion of the digestion, four products remained: Rd-LPE, fatty acyl tails, undigested Rd-PE, and free PE head groups. These groups were separated by thin layer chromatography (TLC). After Rd-LPE being completely dried, SWNTs (arc-deposition, diameter ~1.4 nm) were added to the Rd-LPE at a weight ratio of ~1:5. Then 300 mL of water was added and the solution was probe-sonicated (VC 130 PB, Sonics & Materials) at 8 W for 15 min. The solution was then centrifuged for 3 min at 7,500 RPM and the supernatant then disposed of to remove the SWNT catalysts. As expected, the mixing of SWNTs and Rd-LPE produced a stable and homogeneous solution.

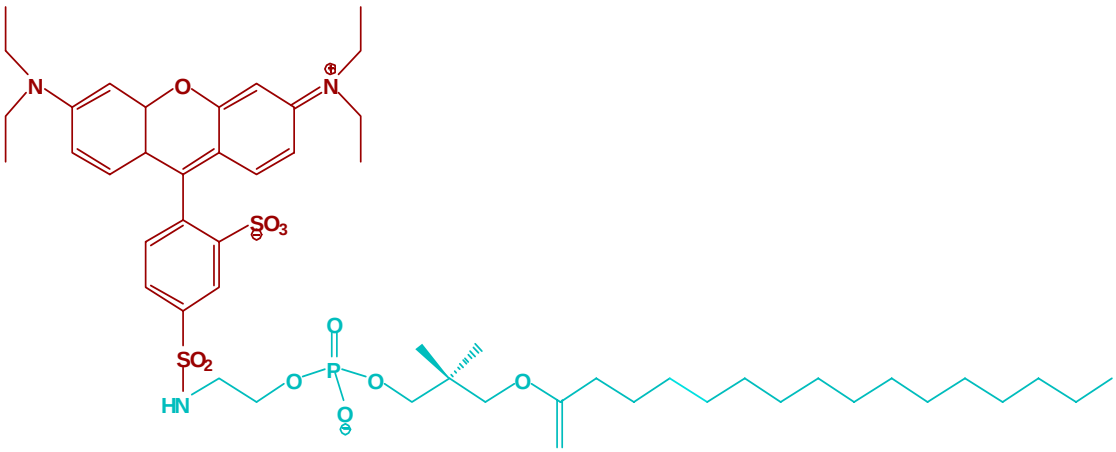

Figure 2.8: Chemical Structure of a Rd-LPE Molecule.

FRET

After obtaining the Rd-LPE-SWNT solution, we noticed a concomitant color change from pink to gray once SWNTs were added to Rd-LPE, indicating the occurrence of FRET. To confirm this, a spectrofluorometer (QM-8/2005, PTI, resolution < 1 nm) was used to measure the fluorescence emission of Rd-LPE and Rd-LPE-SWNT, as shown in the top and bottom panels of Figure 2.9, respectively. The absorption and emission peaks for Rd-LPE were at 571 nm and 583 nm. In contrast, the absorption peak for Rd-LPE-SWNT was blue-shifted to 557 nm and the emission peak was red-shifted to 590 nm. The peak fluorescence intensity of Rd-LPE was more than 8× higher than that of Rd-LPE-SWNT due to strong fluorescence quenching by SWNTs. This phenomenon can be understood from the standpoint of fluorescence resonance energy transfer (FRET) a physical process resulting from induced dipole-induced dipole interactions at a close proximity (< 10 nm). Upon green light excitation, fluorescence emission of Rd-LPE (Figure 2.9 top panel, in purple) is

quenched or drained by the absorption of SWNTs due to their spectral overlap and their nanometric spatial proximity (a Rd-LPE molecule is ~2 nm in length). The blue-shift of the absorbance peak (in orange) and the red-shift of the emission (in purple) in Figure 2.9 further suggest that, due to SWNT absorption, more photon energy is required for fluorescence excitation, while rhodamine emits photons of lower energy. The broadening of the Rd-LPE-SWNT emission spectrum was possibly due to the non-homogeneity of isolated or small bundled SWNTs, as well as the varying physical distances between Rd-LPE molecules in striations and SWNT surfaces. The weak fluorescence emission of SWNTs was unobservable, since the signal was most likely overwhelmed by the fluorescence of free Rd-LPE in solution. By adding chloroform or other amphiphiles to Rd-LPE-SWNT solution, we could remove Rd-LPE from SWNT surfaces and consequently observe the recovery of rhodamine fluorescence (data not shown).

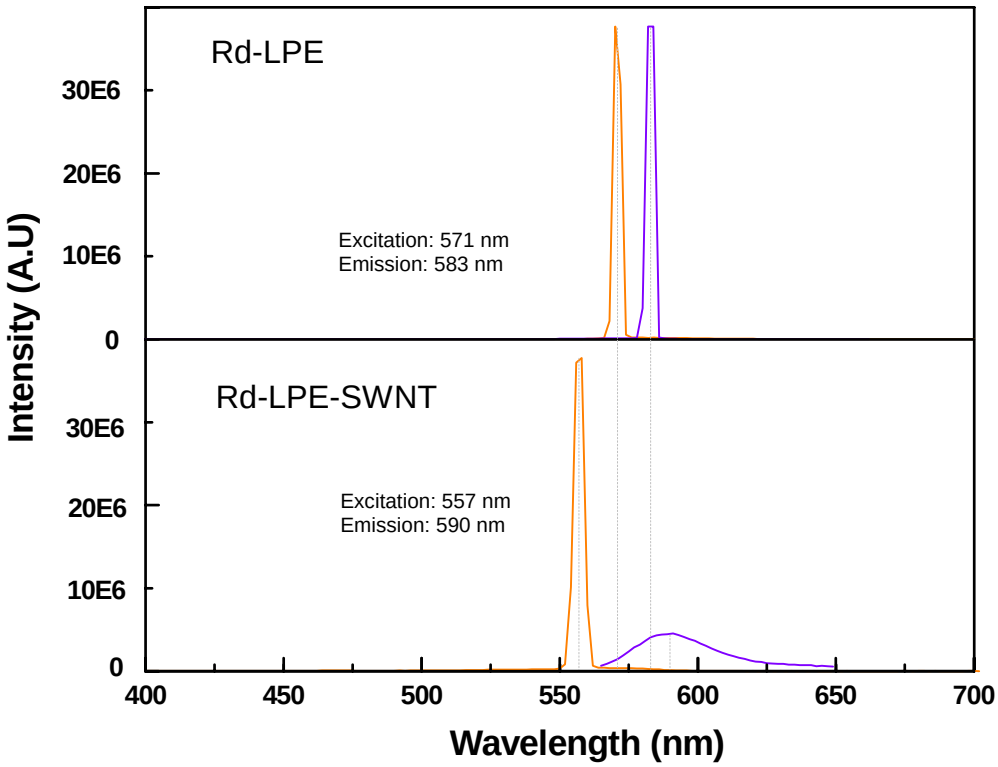

Figure 2.9: Energy Transfer from Rd-LPE to SWNTs. A sharp decrease and broadening of the emission peak (purple) is observed in the bottom panel when compared to the data depicted in the top panel (absorption in orange).

Translocation of Rd-LPE-SWNT across Cell Membranes

The fluorescence quenching and recovery of Rd-LPE upon binding to and dissociation from SWNTs can be utilized for sensing the translocation of SWNTs and their interactions with cell membranes and organelles, a largely unknown area of great interest to researchers in integrating nanomaterials and biological systems. To explore this prospect we imaged the translocation of Rd-LPE-SWNT complexes across MCF7 breast cancer cells. The MCF7 cell line (ATCC) was cultured in DMEM with 1% penicillin streptomycin, 1% sodium pyruvate, and 10% fetal bovine serum. Approximately 10,000 MCF7 cells were

seeded in each (200 μL) of an eight-chambered glass slide and allowed to attach overnight at 37°C with 5% CO_2. Approximately 10 μL of 2 μg/μL of Rd-LPE-SWNT was then added into each chamber and incubated for 0.5, 1, 2, and 3 h, respectively. After incubation, the chambers were washed three times with 1×PBS and kept in PBS for imaging using a confocal fluorescence microscope (LSM510, Zeiss). The excitation source for rhodamine was an Ar^+ laser of 514 nm.

Two controls including Rd-LPE incubated with MCF7 cells for 3 h and Rd-LPE-SWNT without MCF7 cells were imaged. Our first control found no uptake of Rd-LPE without SWNTs (Figure 2.10a), for which we propose the following explanations, all of which indicate that SWNTs are necessary for the translocation of Rd-LPE. Without SWNTs, conical-shaped Rd-LPE might readily form micelles. Alternatively, while endocytosis and passive ratchet diffusion could play significant roles in the translocation of Rd-LPE-SWNT complexes, the hydrophobic moieties of exposed/uncoated SWNTs could prompt interactions with the amphiphilic cell membranes leading to translocation. SWNTs may also affect the electrochemical properties of lipid membranes and the organization of the membrane lipid matrix by varying the lipid/membrane micro-viscosity and rigidity, and therefore facilitating the translocation of Rd-LPE or other drugs into cells. The exchange of Rd-LPE with lipid bilayers of cell membranes needs to be explored for potential applications in molecular signaling. Our second control (Figure 2.10b) without the addition of cells to chamber glass showed no fluorescence from Rd-LPE-SWNT complexes. This observation reinforced the idea that fluorescence is quenched when rhodamine is noncovalently bound to SWNTs.

The time course study in Figures 2.10c-f demonstrates increased rhodamine fluorescence with incubation time. In particular, the red spots appearing on the peripheries of the cell membranes in Figures 2.10c-e suggest some Rd-LPE molecules could be stripped off SWNTs when crossing cell membranes. The cells in Figure 2.10f are largely fluorescent despite being imaged at various focal depths, indicating high translocation efficiency for 3 h incubation and the physical separation of SWNTs and Rd-LPE. We speculate that the strong fluorescence seen in Figure 2.10f is emitted by Rd-LPE molecules dissociated from SWNTs after their translocation across MCF cell membranes. This scheme simulates the ready release of drug loads off their noncovalently bound SWNT transporters and shows promise for developing alternative gene and drug delivery using SWNTs. We noticed that the fluorescence in Figure 2.10f was non-uniformly distributed inside cells while being mostly kept outside cell nuclei. This observation suggests that SWNTs, i.e., the transporters and fluorescence quenchers of Rd-LPE, were selectively stored in cells (e.g., endosomes and lysosomes according to Dai et al.) after their translocation.

Micro-Raman spectroscopy was conducted to probe the presence of SWNTs in cells. The Raman spectra were excited with a 514.5 nm laser line, and the laser power was maintained around 1 mW to avoid sample heating. A Leica microscope equipped with a 50× dry objective (NA=0.75) was used to focus the laser beam. In this experiment Rd-LPE was replaced by LPC to avoid fluorescence overwhelming much weaker Raman signals. The selection of LPC over LPE was because the former offers an SWNT solubility similar to that by Rd-LPE. SWNTs coated by LPC were incubated with MCF7 cells for 2 h, thoroughly washed with 1×PBS before being dried on silicon substrates prior to the measurement. Raman scattered light was collected using an ISA Triax 550 spectrometer equipped with a

liquid-nitrogen cooled CCD. Figure 2.11 shows Raman spectra recorded for pristine SWNTs in isolated form (top), SWNT coated by LPC (middle), and SWNT-LPC incubated with MCF7 cells (bottom). The higher noise level in MCF7 cells is possibly due to the Rayleigh and Raman scatterings of lipids and cell organelles. G-bands around 1590 cm-1 were easily identified in all three cases, indicating the presence of isolated SWNTs in all samples and confirming that SWNTs were indeed translocated into MCF7 cells.

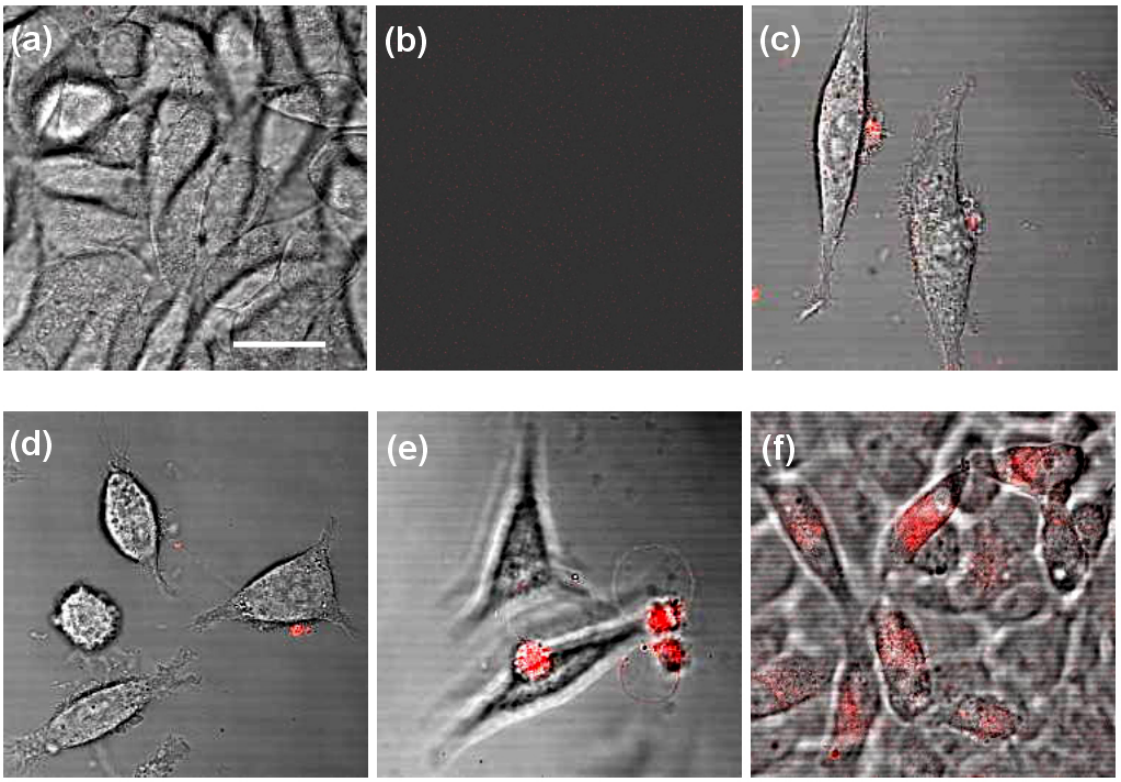

Figure 2.10: Confocal Imaging. (a) Image of control 1 without the use of SWNTs. Rd-LPE was incubated with MCF7 cells for 3 h. No fluorescence was evident, indicating minimal Rd-LPE translocation. (b) Image of control 2 without the presence of MCF7 cells. No rhodamine fluorescence was observed suggesting the tight binding of Rd-LPE to SWNTs resulted in energy transfer. Images (c)-(f) show increased translocation of Rd-LPE across MCF7 cells with incubation times of 0.5, 1, 2, and 3 h. The red spots in the images suggest Rd-LPE were dissociated from SWNTs. Scale bar: 10 μ m.

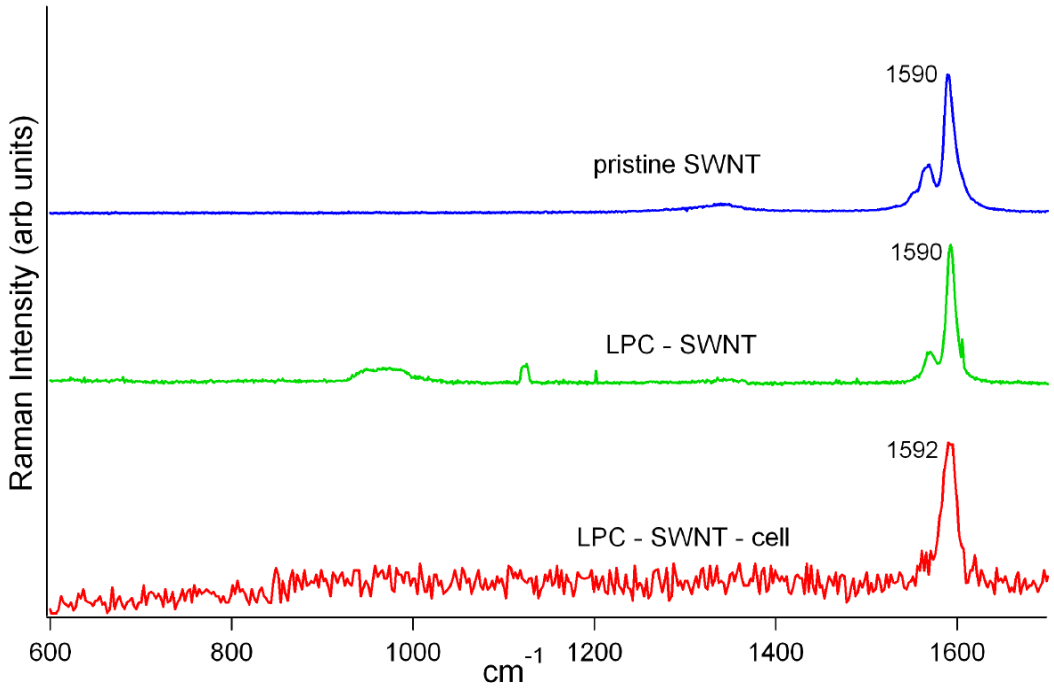

Figure 2.11: Micro-Raman Spectra. Pristine SWNT in isolated form (top/blue), LPC-SWNT (middle, green), and LPC-SWNT in MCF7 cells (bottom, red). The G-bands near 1590 cm-1 are distinct in all cases indicating the presence of isolated SWNTs. Note the high noise level in the bottom trace in the presence of MCF7 cells.

Biomodification of SWNT-LPC by *Daphnia magna*

When introducing nanomaterials into cells or living organisms, the impact of nanomaterials especially the toxicity issue must be examined. In order to understand the fate of carbon nanomaterials in biological systems and in the environment, we used aqueous organism *Daphnia magna* for testing the toxicity of SWNTs. Solubilizing SWNTs with LPC in aqueous solution opens the door for this study.

Acute Toxicity Test

Neonates of *D. magna* used in all bioassays were offspring from an in-house laboratory stock maintained in synthetic laboratory freshwater (moderately hard freshwater) prepared as described by the U.S. EPA. (REF) Synthetic freshwater was aerated overnight prior to use in bioassays. Test solutions were prepared by adding appropriate volumes of SWNT-LPC stock (2 g/L) to synthetic freshwater to achieve the desired test concentrations of 0, 2.5, 5, 10, and 20 mg/L.

Static renewal acute toxicity tests were performed by exposing *D. magna* less than 24 h in 100 mL polyethylene cups containing 50 mL test solutions at 25˚C. Five replicates were tested per treatment each containing five neonates. Mortality was observed at 24 h intervals, and all living organisms were transferred to test chambers containing fresh test solutions. After daily transfer, organisms were fed a diet of algae (Selenastrum capricornutum) and yeast trout chow. Tests were conducted for 96 h. No mortality was observed at test concentrations of 0, 2.5, and 5 mg/L SWNT-LPC (Figure 2.12). Mortality of 20% and 100% were observed in the 10 mg/L and 20 mg/L SWNT-LPC test concentrations, respectively. Black precipitates formed in the test cups within 24 h of the beginning of the exposure and within the 24 h following test solution renewal. These precipitates were observed not only sticking to the polyethylene exposure cups but also adhering to the external surface of the daphnids. In some cases, the clumping was significant enough to prevent ambulation of the daphnids through the water column and caused them to sink to the bottom of the exposure cups.

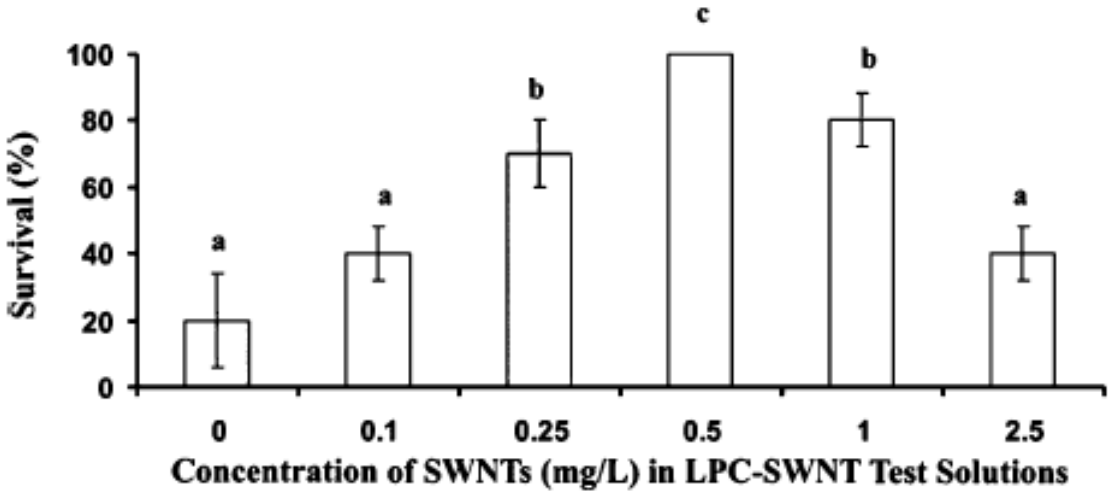

Figure 2.12: Mean Percent Survival of Daphnia magna. Exposed to SWNT-LPC under starvation conditions (no algae-YTC food) for 96 h.

Daphnid Uptake of SWNT-LPC

During toxicity study, black precipitates formed down the cup with daphnia in. This might be because the daphnia were able to stripe out the LPC on the surface of SWNTs and the SWNTs re-aggregate once they lost the LPC coating. Micro-Raman spectroscopy was used to confirm uptake of the SWNT-LPC by *D. magna* and to confirm that the black precipitates were indeed composed of SWNTs.

Raman spectroscopy is a sensitive light scattering technique that probes the intrinsic properties (e.g., chemical composition and molecular structure) of a sample under study. The G-band of SWNTs, upon laser excitation for example, represents the graphite-related vibrational modes in the tangential directions upon excitation. The analysis was carried out according to the methods of Jorio et al. [57] Briefly, *D. magna* (<24 h old) were exposed to SWNT-LPC as described under Acute Toxicity Test. After 1 h, micro-Raman spectroscopy

was conducted to probe the presence of SWNTs in exposed and unexposed daphnids. The Raman spectra were excited with a 514.5 nm laser line, and the laser power was maintained around 1 mW to avoid sample heating. A Leica microscope equipped with a 5× dry objective was used to focus the laser beam. The Raman scattered light was collected using an ISA Triax 550 spectrometer equipped with a liquid-nitrogen cooled CCD. After 20 h of exposure, significant amounts of black precipitate had formed in the cups. Samples of this precipitate were also collected and analyzed for the presence of SWNTs using micro-Raman spectroscopy.

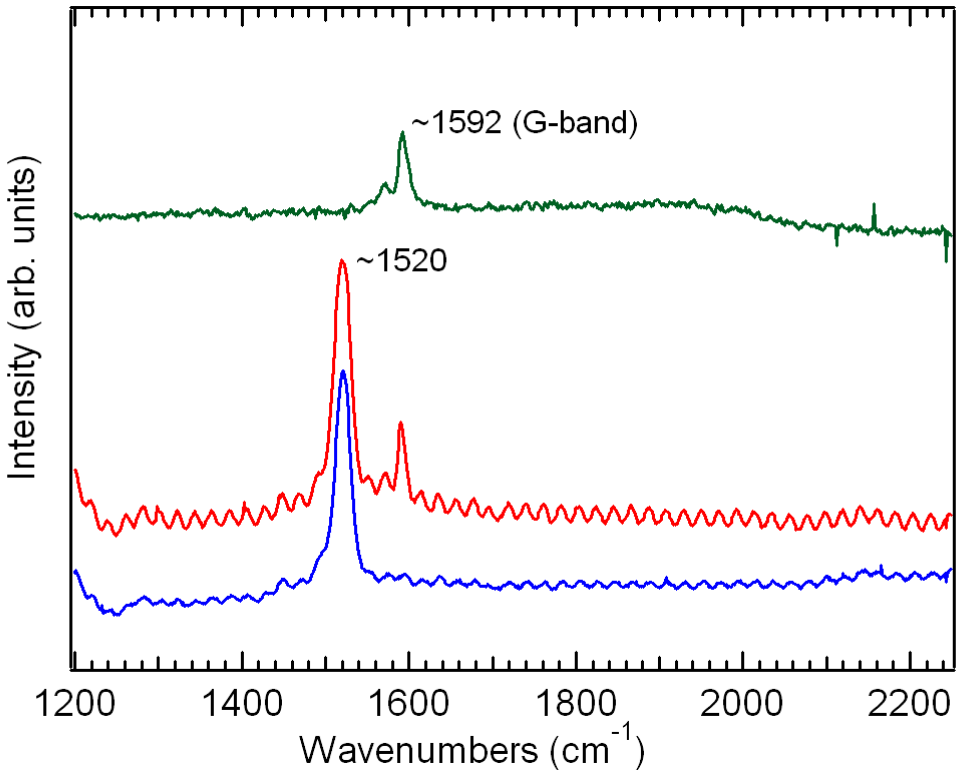

Figure 2.13: Raman Spectra. Recorded for Daphnia magna after exposure to SWNT-LPC for 1 h (red line), control unexposed *D. magna* (blue line), and precipitates from exposure cup collected 20 h after exposure initiation (top green line). G-bands around 1592 cm-1 were identified for both red (exposed *D. magna*) and green curves (precipitates), indicating the presence of SWNTs in these two cases. No G-band was found for the blue curve. The strong peaks at 1520 cm-1 are likely from the daphnids themselves.

SWNT-LPC as Food Source

We hypothesized that *D. magna* may be able to utilize the LPC portion of ingested SWNT-LPC as a food source. To test this hypothesis, *D. magna* (<24 h old) were exposed to graded, sublethal concentrations of SWNT-LPC (0, 0.1, 0.25, 0.5, 1, 2.5 mg/L) in moderately hard synthetic freshwater as previously described under Acute Toxicity Test. Ten replicate cups per concentration (each containing five *D. magna*) were used. Five cups from each

concentration were fed a mixture of Selenastrum-YTC daily, while the remaining five cups were not fed the algae-YTC mixture. This insured that the only source of nutrition in the test cup would come from the test solution (containing SWNT-LPC). Mortality was counted every 24 h over a 96 h period, and test solutions were renewed daily.

Microscopic Imaging

D. magna were exposed to SWNT-LPC in moderately hard synthetic freshwater as described in previous sections. Daphnia were not fed to ensure that their gut tracts were clear of any food material other than SWNT-LPC. Two to three live *D. magna* were transferred to a single chamber of a LabTek 8-well chamber slide. A 1% agarose (in synethetic freshwater) solution was added to the chamber to immobilize the daphnid, and the slide was cooled for 10 min at 4°C to allow the gel to solidify. Micrographs were taken on a Zeiss 510 laser scanning confocal fluorescent microscope.

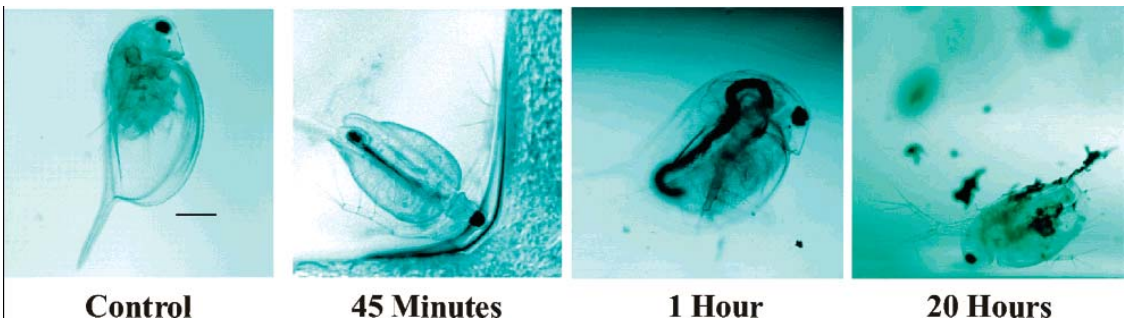

Figure 2.14: Time Course Micrographs of *Daphnia magna* Exposed to SWNT-LPC

Figure 2.14 shows a daphnid exposed to SWNT-LPC for different exposure times. As shown in control, the daphnid had a clear gut track without any food inside. After 45 min

of exposure, the gut track was half filled with black particles which are the aggregated SWNTs. One hour's exposure gave the *Daphnid* a full gut track. Interestingly, after 20 h of exposure, the *Daphnid* was still alive and SWNT aggregates were found not only in the gut track, but also outside the body and on the skin of the *Daphnid*. We believe the *Daphnid* was able to excrete the SWNTs and retook the soluble SWNT-LPC. The excreted SWNTs lost the coating of LPC and reaggregated back to form bundles. Some of the SWNT aggregates were attached to the hydrophobic surface of the *Daphnid*.

The biomodificaiton of *Daphnia* represents one possible response of biological or environmental system to carbon nanomaterials. After LPC being utilized as a food source, the SWNTs were no longer soluble and their aggregates clung to the *Daphnia* skin could reduce the mobility of this organism. The aggregates which settled down into the soil would affect plants, bacteria, and microbial. More research needs to be done in this direction to evaluate the impact of nanomaterials on the environment.

CHAPTER THREE

FULLERENE FOR IMAGING AND SENSING

C_{70} is the shortest "SWNT" and one of the smallest nanoparticles. The diameter of C_{70} is ~0.8 nm. The hydrophobic nature of C_{70} offers opportunities to interact with biological systems. In order to bridge C_{70} with biological systems, the first step is to solubilize C_{70} in aqueous solutions. Gallic acid, an organic phenol, is well known for its anti-oxidant and anti-cancer properties. With three phenol groups and one carboxyl group sticking out of one benzene ring, gallic acid is polar and is water soluble. Furthermore, the benzene ring of gallic acid provides an opportunity to pi-stack with molecules which also have carbon rings on the exterior, such as C_{70}. Based on this understanding, we successfully solubilized C_{70} by gallic acid in aqueous environment. The solution emitted green fluorescence which could be used to label biological systems at cellular, tissue and the whole living organism levels. Also we found that the fluorescence of the complex C_{70}-gallic acid was much stable than commercial dyes such as calcium AM under the irradiation of light. Through confocal fluorescence microscopy, we observed the first real-time translocation of C_{70}-gallic acid across HT-29 cancer cells.

Solubilizing C_{70} in Aqueous Environment by Gallic Acid

C_{70} (MW: 840 g/mol) and gallic acid (MW: 170 g/mol) were mixed in distilled water by weight ratios of 1:5, 1:10, and 1:20, corresponding to molar ratios of 1:25, 1:50, and 1:100, respectively. The mixtures were probe-sonicated (VC 130 PB, Sonics & Materials) at 8 W for 30 min and placed at room temperature for 3 days. This time frame was needed to enable

the intermolecular interaction between C_{70} and gallic acid. The mixtures turned into a stable and homogenous solution and emitted green color.

The structure of C_{70}-gallic acid is believed to be formed via pi-stacking. Figure (3.1 top) illustrates one possible complex structure, where both steric hindrance and repulsion between gallic acid molecules (negatively charged) exist to prevent perfect coating of C_{70}. In addition, the hydrogen bonding between the oxygen and hydrogen atoms within gallic acid molecules may also contribute to the supramolecular structure, which renders gallic acid molecules caging around the fullerene molecules. Due to the repulsion between gallic acid molecules, multiple C_{70} molecules might be enclosed by one gallic acid cage since it would be energetically unfavorable otherwise.

TEM imaging was conducted to measure the size distribution of C_{70}-gallic acid complexes (Figure 3.1 bottom). C_{70}-gallic acid solution was first filtered through a centrifugal filter device (MWCO 3,000) to remove large clumps of C_{70} particles and dialyzed for 12 h using a membrane (MWCO 500) to remove free gallic acid molecules. The solution was then placed on a holey carbon grid for 1 min and the excess drawn off with filter paper. The grid was negatively stained with a 2% uranyl acetate solution for 1 min. Images were recorded at a magnification of 600,000× with a Hitachi 7600 transmission electron microscope at 100 kV.

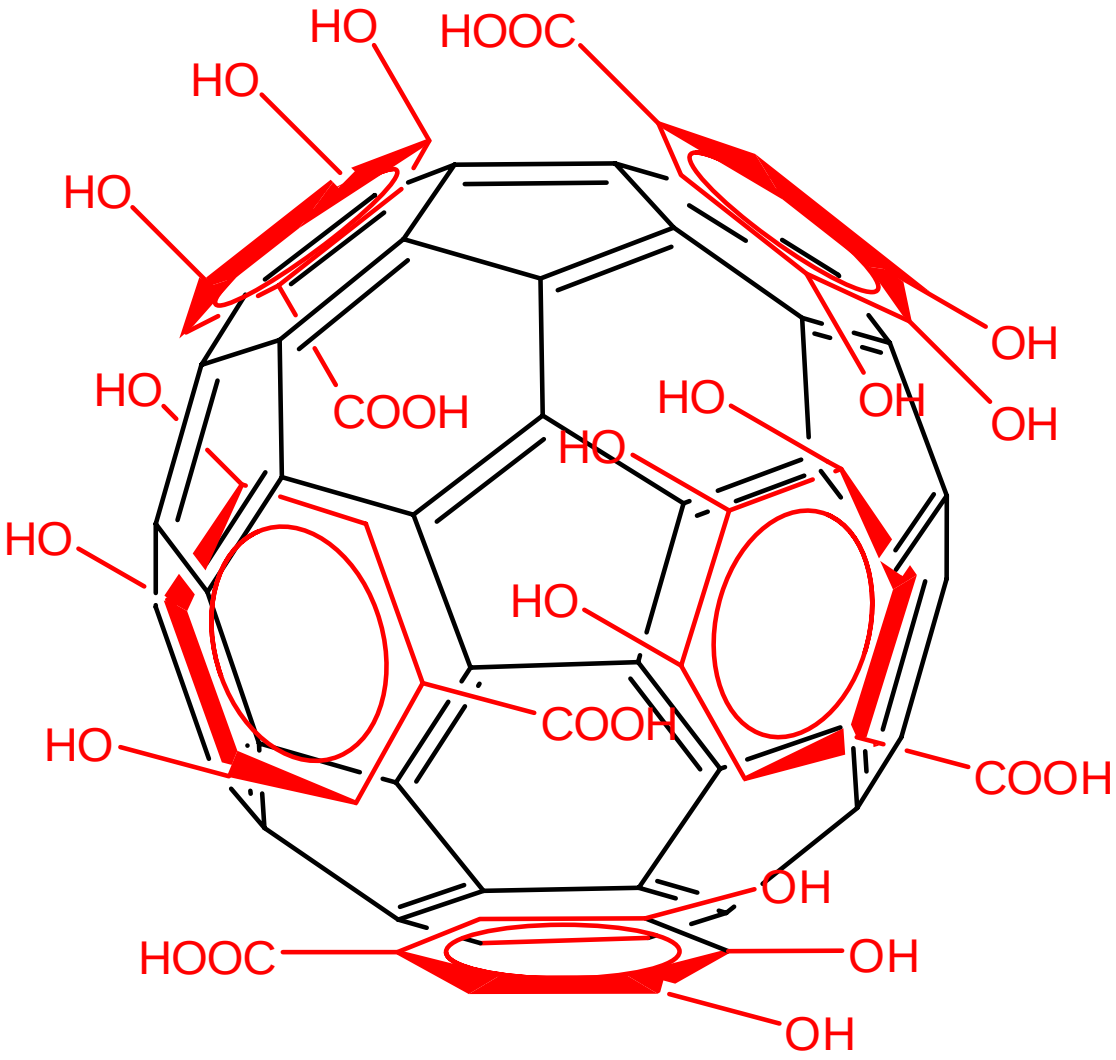

Figure 3.1a: Predicted Structure of C_{70}-gallic acid Complex

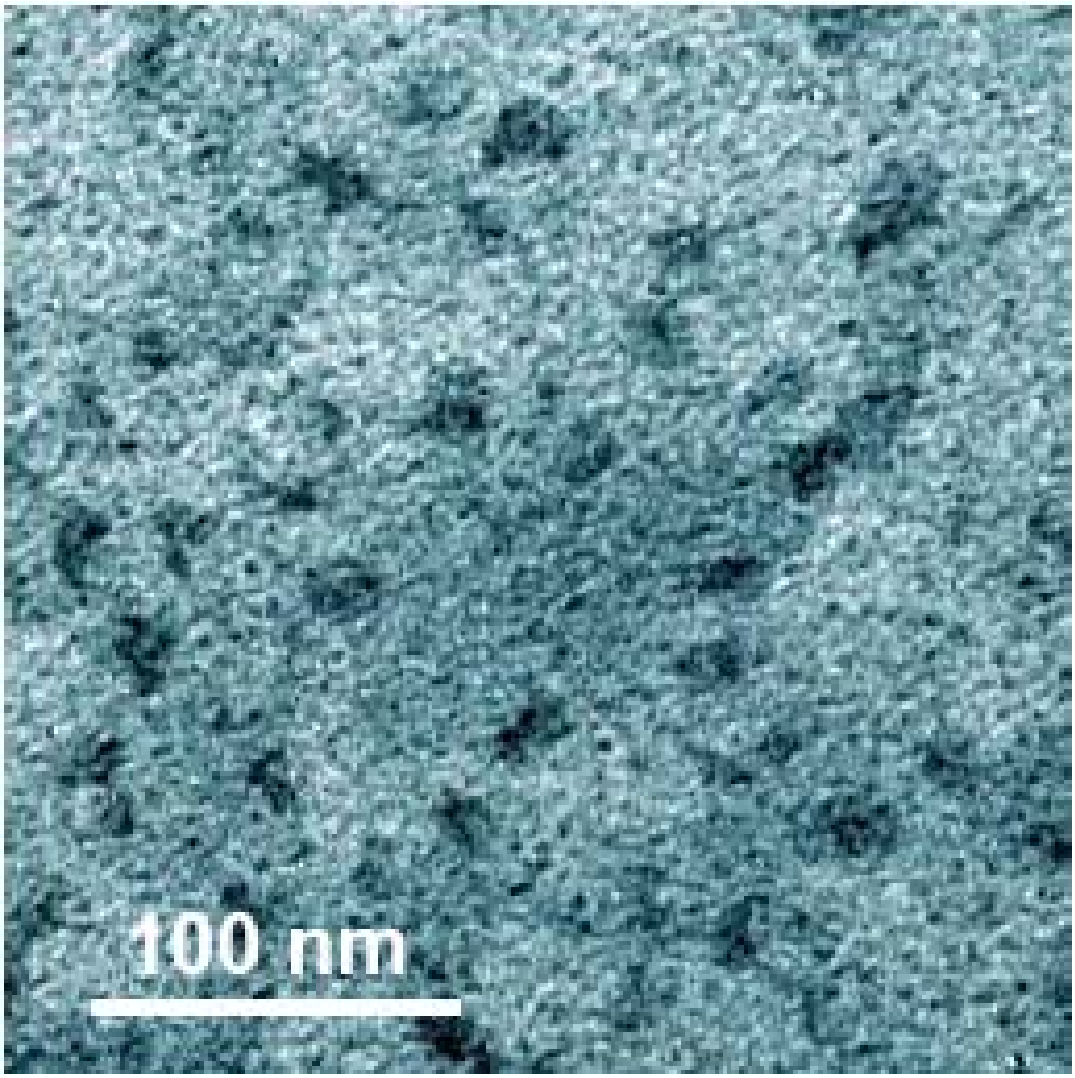

Figure 3.1b: C_{70}-gallic acid Complex TEM Image

Absorbance of gallic acid only and C_{70}-gallic acid solution were then measured by Biomate Spectrophotometer at room temperature. The solubility curves of C_{70} were obtained based on the absorption intensity at 384 nm, where gallic acid had minimal absorbance

(Figure 3.2a). The solubility curves were largely linear until a plateau was reached at 1 mg/mL (Figure 3.2b).

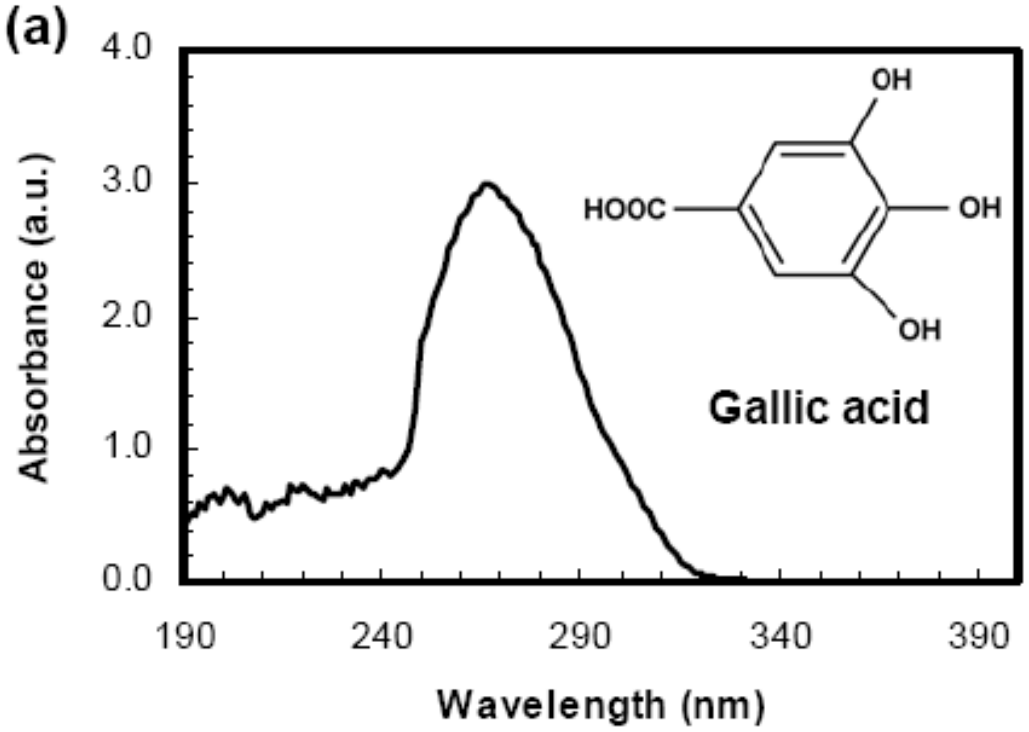

Figure 3.2a: Absorbance of gallic acid only (structure see inset)

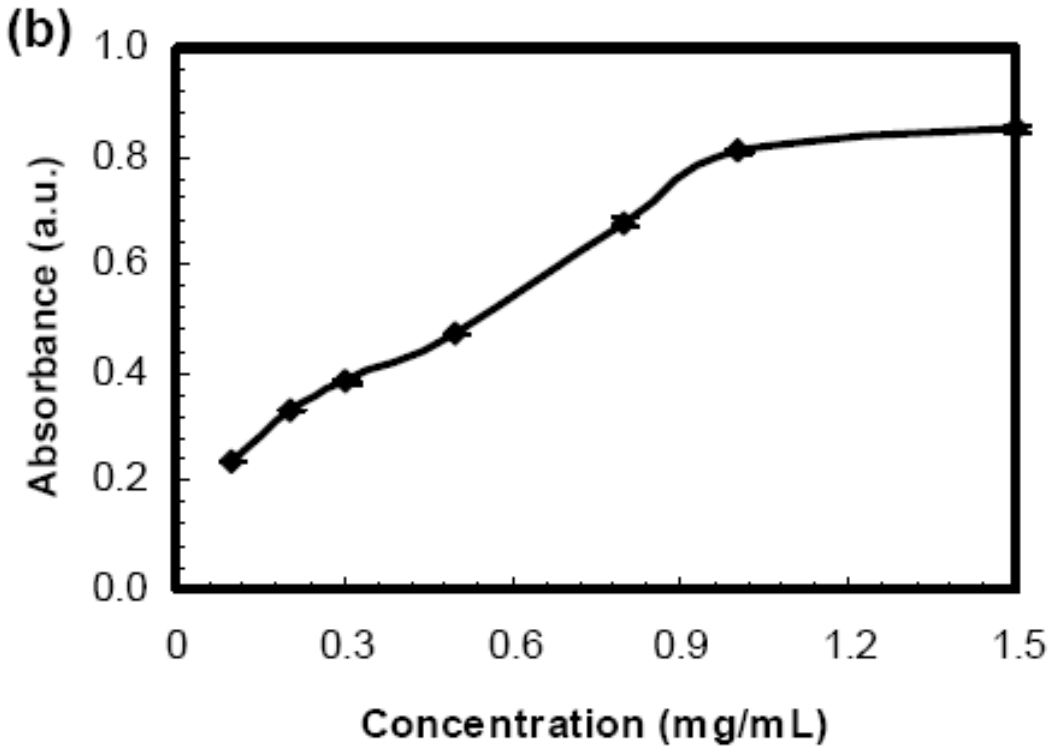

Figure 3.2b: Absorbance-Concentration Relation

Fluorescence measurement was conducted using a spectrofluorometer (QM-8/2005, PTI, resolution < 1 nm). (Figures 3.3a and b). The weight ratio of C_{70} to gallic acid was varied from 1:5 to 1:20, corresponding to a molar ratio of approximate 1/25 to 1/100. As a control, gallic acid of equal amount to the sample yielded only weak fluorescence when excited at 488 nm (grey curve in Figure 3.3a). In contrast two distinct fluorescence peaks were observed at ~540 nm and 736 nm when the sample (1:5, dark red curve) was excited at 488 nm and 690 nm, respectively. This confirms that the fluorescence signals observed at 540 nm and 736 nm were emitted by C_{70} not gallic acid. As shown in Figure 3.3a,

centrifugation at 7.5×10^3 RPM for 3 min did not significantly alter the broad fluorescence peak at 540 nm while markedly reducing the narrow peak at 736 nm (blue curve in Figure 3.3a). This suggests the fluorescence peak at 736 nm was mostly emitted by poorly solubilized C_{70} molecules. This result is similar to that observed for C_{60}-pyridine solutions, where fluorescence peaks at 440 nm, 575 nm, and 700 nm were assigned to C_{60} nanoparticles, C_{60} lace-like clusters, and C_{60} microbulks, respectively [58]. Consistently, the cyan curve (1:20) in Figure 3.3b exhibits a relatively smaller peak at 736 nm as compared to the orange curve (1:10), possibly due to the higher concentration of gallic acid and therefore improved C_{70} solubility.

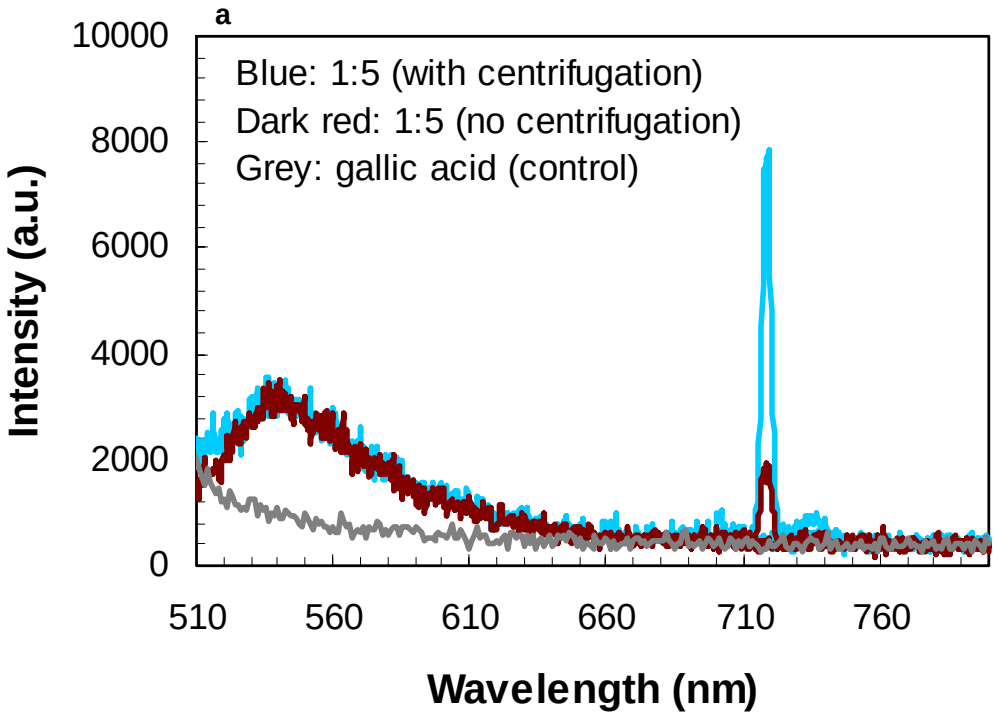

Figure 3.3a: Fluorescence Intensity vs. Wavelength for C_{70}-gallic acid. The ratio of C_{70}-gallic acid was set at 1:5 and the concentration of C_{70} was 0.1 mg/mL prior to centrifugation (blue). The prominent fluorescence peak at 736 nm is greatly reduced after centrifugation (from blue to dark red curve). The fluorescence of gallic acid is shown in grey as control

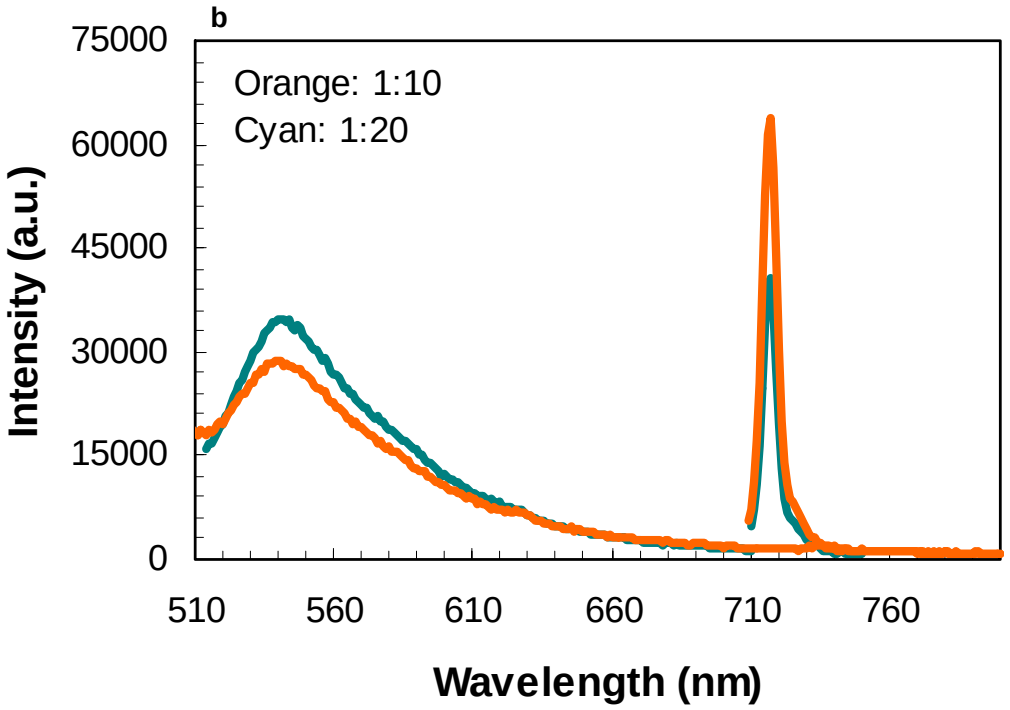

Figure 3.3b: Fluorescence Intensity vs. Wavelength for C_{70}-gallic acid of Different Ratios. The concentrations of C_{70} were 1 mg/mL for both C_{70}-gallic acid of 1:10 (orange) and 1:20 (cyan). No centrifuged.

Fluorescence Labeling of C_{70}-gallic acid

Utilizing the green fluorescence of C_{70}-gallic acid, we conducted imaging of Chinese hamster Ovary (CHO) cells and living organism *Daphnia magna* (water flea). As shown in Figure 3.4, both the interiors and outer surfaces of the cells and the Daphnia were strongly fluorescent when excited by an Ar^+ laser at 488 nm, indicating the efficient translocation of C_{70}-gallic acid across cell membranes. However the green fluorescence was mostly excluded by the cell nuclei (Figure 3.4a) possibly due to the relatively large sizes of C_{70}-gallic acid and their dissociation dynamics in the cellular environment. In Figure 3.4b the head of the

Daphnid with a single compound eye is visible and the swimming appendages can be seen extended from the cephalothorax surrounding the crustacean's body. In this experiment the ingestion of C_{70}-gallic acid by Daphnia and their consequent permeation into tissues is possible. However since labeling of *Daphnia* by C_{70}-gallic acid could be done within minutes, we believe this internalization route contributed less than the permeation of the nanoparticles through membranes.

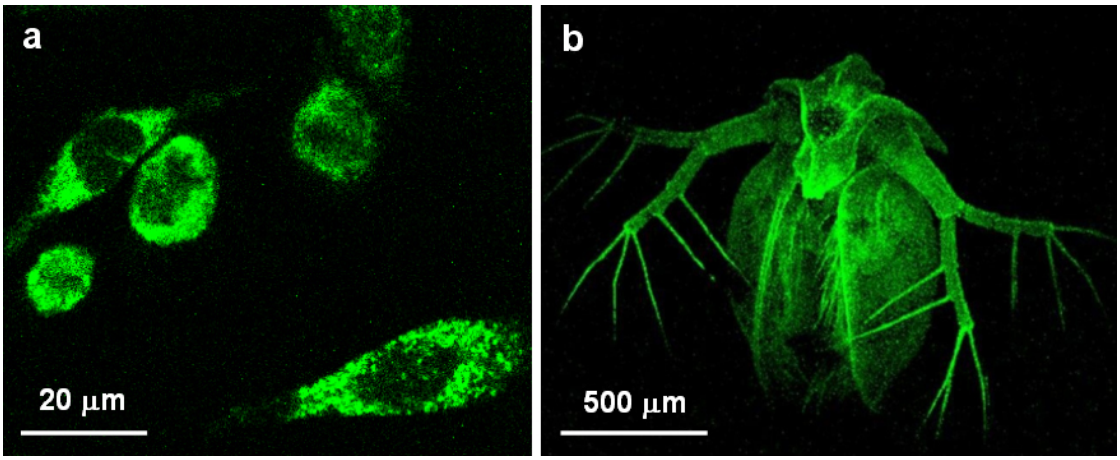

Figure 3.4: Confocal Fluorescence Images of C_{70}-gallic acid Labeled a) CHO Cells and b) A Living *Daphnid*, excited by an Ar^+ laser at 488 nm.

In comparison with calcein AM, a routine stain for examining biological samples, the labeling of C_{70}-gallic acid was less selective (Figure 3.5a vs. 3.5c) and far more resistant to irradiation (Figure 3.5b vs. 3.5d) when living oyster tissues were imaged. Calcein AM is known to only fluoresce after its AM moiety is cleaved off by intracellular esterases. For that matter calcein AM usually requires an incubation time of ~20 min or longer. In comparison cell or tissue labeling with C_{70}-gallic acid was almost instantaneous. In addition, while calcein

AM can only be used for viable samples due to its peculiar fluorescence mechanism, C_{70}-gallic acid readily labels both living and fixed cells with almost the same efficiency. The resistance of C_{70}-gallic acid to irradiation allows these nanoparticles to be far more effective than calcein AM for examining large tissues and organisms. Figure 3.5 shows a comparison of the labeling using C_{70}-gallic acid and calceim AM. Under the same laser exposure, the fluorescence of C_{70} (b) is much stable than the fluorescence of calceim AM (d).

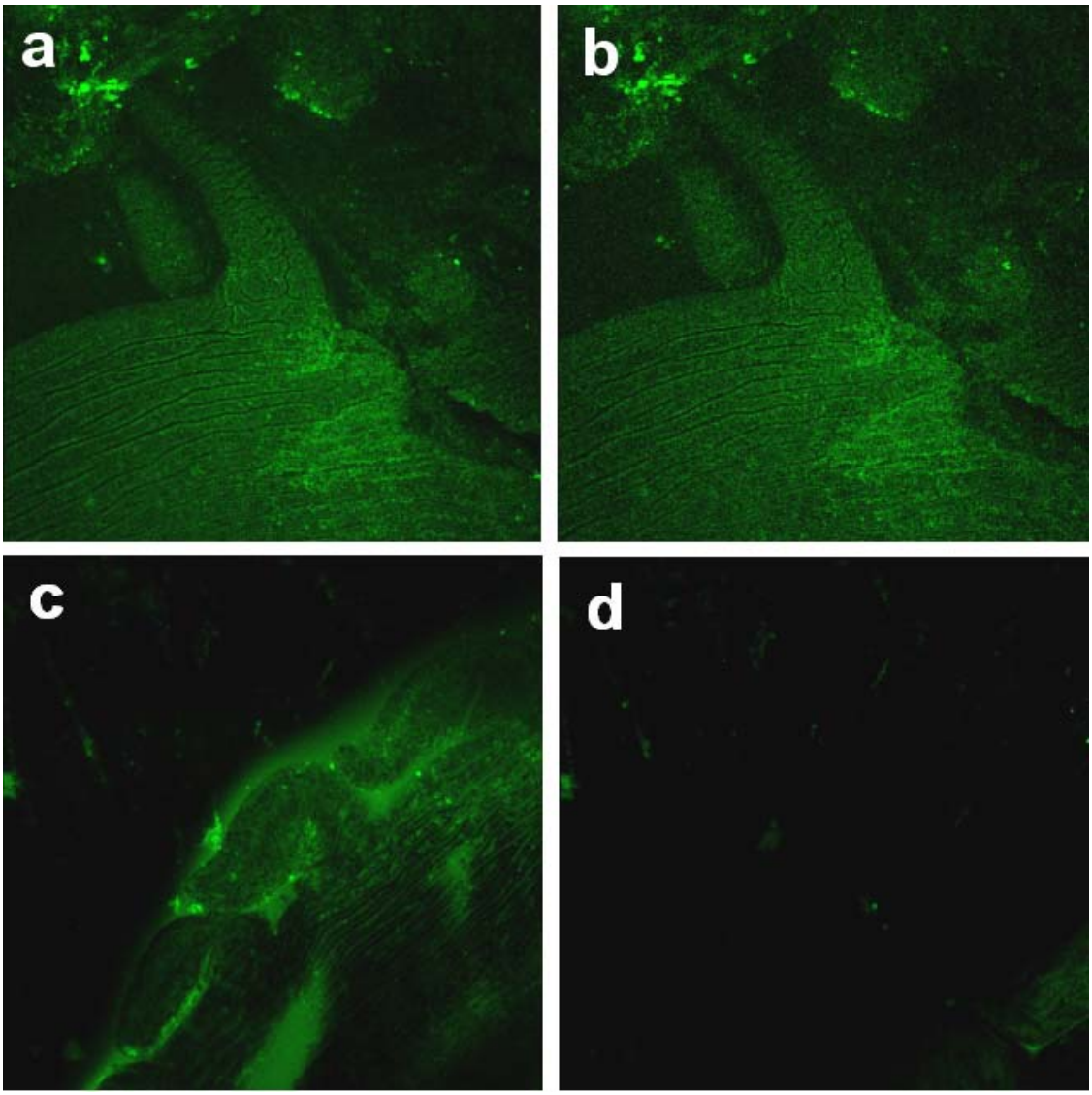

Figure 3.5: Fluorescence Imaging of Labeled Tissue. C_{70}-gallic acid Labeled living mantle tissue a) before and b) after 4 min of Ar^+ laser irradiation. In contrast, c) and d) are calcein AM labeled living mantle tissue c) before and d) after 4 min of laser irradiation.

Translocation of C_{70}-gallic acid inside Cancer Cells (HT-29)

The translocation property of C_{70}-gallic acid was tested in HT-29 colon cancer cell lines. The HT-29 cell lines (ATCC) were cultured in DMEM with 1% penicillin streptomycin, 1% sodium pyruvate, and 10% fetal bovine serum. Approximately 10,000 HT-29 cells were

seeded in each (200 uL) of an eight-chambered glass slide and allowed to attach overnight at 37°C with 5% CO_2. The HT-29 cells were fluorescently labeled by a lipophilic dye DiI (Ex/Em: 549/565 nm, Molecular Probes). The dye only labeled the cell membranes which appeared in the microscopic images as "rings" surrounding the cells. Approximately 20 uL of 0.1 mg/mL C_{70}-gallic acid was added in each chamber well right before the images were taken. The time lapse between each consecutive image was 5 min and all the microscope parameters of the confocal, like laser intensity, pinhole range, detection gain and focus plane, were kept unchanged during the real-time imaging.

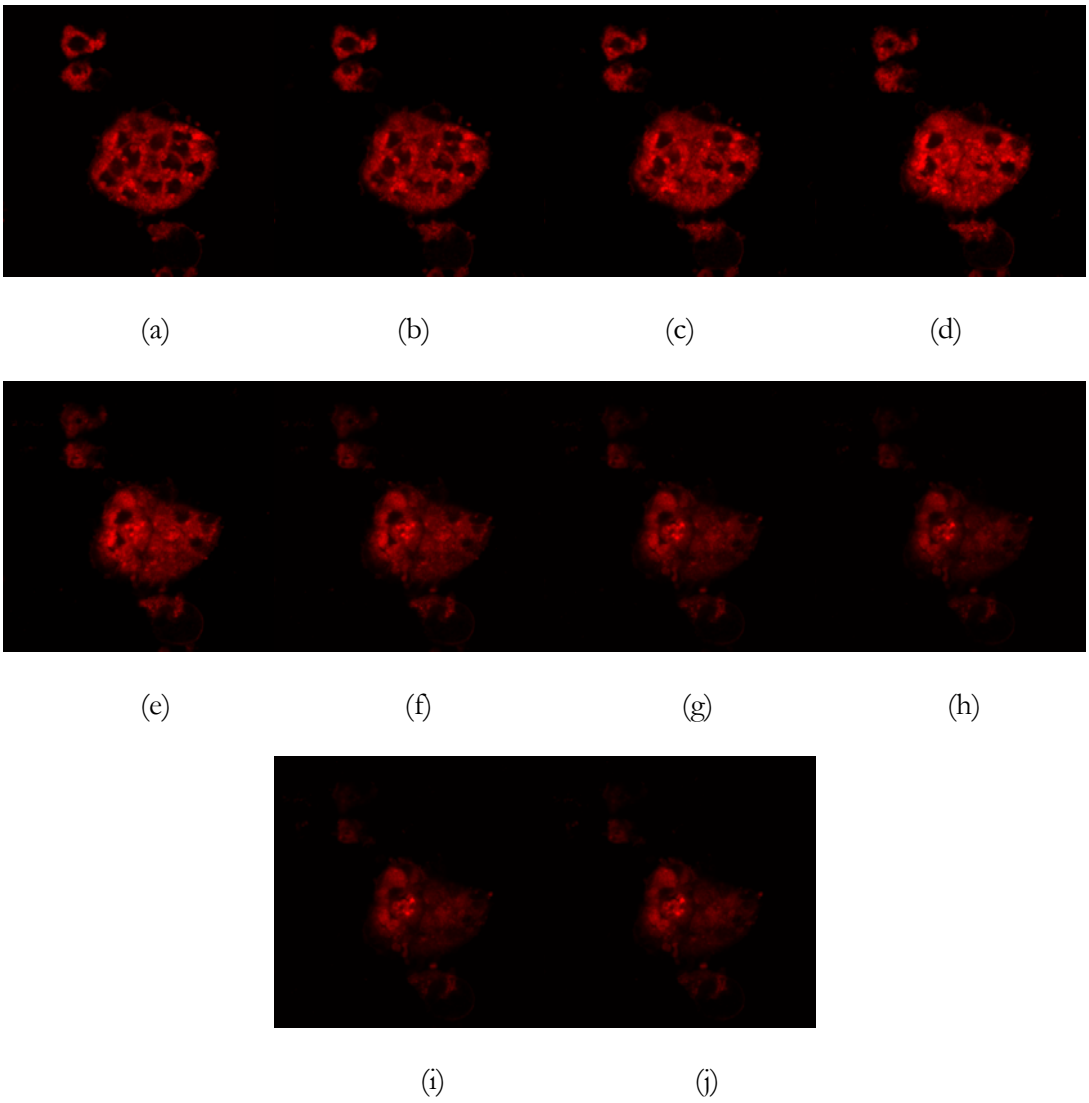

Figure 3.6: Conformational Changes of HT-29 Cell Membrane, due to the translocation of C_{70}-gallic acid. The time lapse between each consecutive image is 5 min.

Figure 3.6 shows the change of fluorescence of HT-29 cells due to the translocation of C_{70}-gallic acid across the DiI-labeled cell membranes. Because the focus plane does not change, the reductions of the "rings" indicate the pushing of cell membranes by the nanoparticles into the focus or the wrapping of C_{70}-gallic acid complexes by DiI-labeled

phospholipids after their translocation. Further investigations are needed to confirm that the C_{70}-gallic acid complexes actually translocated into the cytosol of the HT-29 cells.

The number of C_{70}-gallic acid in each sample chamber, N_{nano}, can be estimated as

$$N_{nano} = [C]*V/W, \quad (3\text{-}1)$$

where [C] is the concentration of C_{70}-gallic acid (0.1 mg/mL), V the volume of the solution added to each chamber (20 uL), and W the average weight of each C_{70} aggregate (3.5×10^{-20} g) estimated based on TEM imaging (Figure 3.1). Assuming the cells are hemispherical due to their adhesion to the chamber glass, we can calculate the total number of the nanoparticles interacting with each cell, N_{cell}, as

$$N_{cell}=N_{nano}*4/3Pi*r^3/2/V, \quad (3\text{-}2)$$

where r is the average radius of each cell (5 um) based on confocal imaging. The surface area of each seeded cell A can be estimated as

$$A = 4pi*r^2/2. \quad (3\text{-}3)$$

The physical pressure P exerted by the nanoparticles on each cell surface can be calculated as 1.7×10^{-7} kg/m^2 or ~$1.7x10^{-11}$ atm based on formula $P=N_{cell}*W/A$.

CHAPTER FOUR

CONCLUSIONS AND FUTURE WORK

In Chapter two, we have discovered an efficient method of solubilizing SWNTs in aqueous solution using zwitterionic lipids. The interaction between lipids and SWNTs largely depends on hydrophobic interactions. The fluorescence energy transfer within the supramolecular assembly of Rd-LPE-SWNT makes it possible to detect the translocation of SWNTs through cancer cell membranes. The lack of rhodamine fluorescence in the extracellular space suggests the high binding efficiency and the stability of the Rd-LPE-SWNT complexes prior to their translocation. In contrast, the presence of strong rhodamine fluorescence in the intracellular space simulates the direct and efficient release of drug loads (i.e., Rd-LPE in this case) from SWNT transporters, a feature unavailable from covalent methods and is desirable for gene and drug delivery. The non-uniform distribution of rhodamine fluorescence inside cells suggests the inhomogeneous distribution and storage of SWNTs in cellular environments which deserves further investigation. Since lysophospholipids, lysophosphatidic acid and sphingosine 1-phosphate can be used as receptors for signal transduction and the head groups of lysophospholipids offer great versatility in biofunctionalization of genes and drugs, our method provides an "optical switch" for detecting the real-time interaction of SWNTs and biomolecules and suggests the use SWNTs as energy quenchers for biosensing and transporters for nanomedicine.

Considering the environmental effect of SWNTs, we found that *D. magna* were able to ingest the solubilized nanotubes through normal feeding behavior and utilize the LPC coating as a food source. After the daphnids digesting the LPC, SWNT lost the coating and

accumulated in the gut track. Daphnids were able to excrete the clumps of SWNTs out the body and retake the soluble SWNTs in the solution. The excreted SWNTs, without the coating of LPC, were no longer water soluble and, thus, precipitated out of the water column. Our data demonstrates the biomodification of a coated nanomaterial by an aquatic organism. Moreover, this modification resulted in a significant alteration of the physical properties of the material resulting in clumping and precipitation of solubilized SWNTs. These results indicate that ecologically important species may have dramatic effects on the physical properties of engineered nanomaterials and affect their fate in the environment. More attention need to be paid is that some of the accumulated SWNTs stuck on the external surface of *D. magna* and may lead to a potential effect of toxicity. In several bioassays, we observed sufficient accumulation of SWNTs to prevent the organisms from moving through the water column and in some cases, enough to weigh them to the bottom of the exposure chamber. Accumulation at such high levels would almost certainly result in a decreased ability to feed and deleterious chronic effects. It seems likely that the extra mass adhered to the organism would have energetic effects in the long-term, resulting in decreased growth and decreased or delayed reproduction. Studies of these types of effects resulting from chronic exposure as well as studies investigating potential cellular toxicity from chronic exposure are needed.

In Chapter three, a supramolecule of C_{70}-gallic acid was assembled via pi-stacking and its solubility afforded by the three hydroxyls and one carboxyl of each gallic acid molecule. In addition, gallic acid molecules could cage around C_{70} molecule(s) via hydrogen bonds to elicit an improved solubility. According to our TEM study each C_{70}-gallic acid complex usually encased multiple C_{70} molecules due to their mutual *van der Waals* bonding.

In water solutions hydrophobic and electrostatic interactions also take place to reinforce the interactions between C_{70} molecules. With consecutive filtrations to remove free gallic acid and larger C_{70} or C_{70}-gallic acid aggregates, the average diameter of C_{70}-gallic acid complex was found to be ~20 nm.

The solution of C_{70}-gallic acid exhibited light green color in water and was stable for weeks at room temperature. Moreover, the green color is due to the fluorescence of soluble C_{70}. The C_{70}-gallic acid complexes emit multiple fluorescence bands in visible and in near infrared and we have assigned the 540 nm band to well solubilized C_{70}. The mechanism of the robust fluorescence of C_{70}-gallic acid in water is unclear but is speculated to be due to the degenerated electronic states, reduced symmetry, and the rapid intersystem crossing of the C_{70}. Utilizing the fluorescence of C_{70}-gallic acid we have performed imaging from the cellular to the living organism level. We have shown that the fluorescence of C_{70}-gallic acid is more resistant to photobleaching and far less selective to the state of biological samples than calcein AM. The free radical generation of pristine fullerenes is of some concern, but in principle it could be counterbalanced by gallic acid which is a powerful antioxidant. Since gallic acid is also an anticancer agent and can be further functionalized to incorporate disease-specific antibodies, C_{70}-gallic acid could potentially find broad applications in biosensing, in vivo imaging, therapeutics, and drug delivery.

In short, my MS research can be summarized as the following.

- I have characterized SWNT solubility in aqueous solutions of different amphiphilic molecules (DOPA, SDS and LPC), and studied the stability of these solutions by varying parameters such as temperature, pH, and ionic strength. Based on the absorbance peak values of SWNT (done by

spectrophotometry), SWNT suspensions became less stable with the decrease of pH value or the increase of ionic strength. However, these suspensions showed no dependence on temperature within the range of 4-96°C;

- I have obtained a supramolecular complex of SWNT-Rd-LPE in aqueous solution. Based on the mechanism of FRET, I conducted cell imaging using confocal fluorescence microscope and detected the binding and releasing of Rd-LPE with respect to its SWNT transporter. These results indicate that SWNT can act as an effective lipid transporter across cancer cell membranes;
- I have conducted confocal fluorescence imaging to show the uptake of SWNT and the biomodification of SWNT-LPC by *D. magna* through normal feed behavior. The excreted SWNT by *D. magna* indicates this living organism can biomodify the physical property of SWNT-LPC which may lead to daphnia mortality; and
- I have successfully solubilized C70 using gallic acid and detected its green fluorescence using fluorometer. This fluorescence has been found to be more resistant to photobleaching than commercial dye calcein AM. I have cultured HT-29 cell lines and measured the real-time translocation of C_{70}-gallic acid across the cell membranes.

Future work will be conducted in the following areas. One direction would be the biofunctionalization of lipids or gallic acids, which are used for solubilizing nanomaterials and for targeting at specific diseases. In order to cooperate more different types of nanomaterials with the biological systems and understand their impact, another direction would be to use modeling to predict solubility based on the molecules' hydrophobicity and

morphology. Although our method of solubilizing SWNTs using lysophospholipids rendered great solubility, it is nonpractical for us to conduct the environmental studies of nanomaterials based on this model. Natural organic matter (NOM) is the most common content in all water sources in the environment, and understanding NOM interacting with discharged carbon nanomaterials would be far more relevant for eliciting the environmental impact of nanomaterials.

REFERENCES

1. M. M. J. Treacy, T. W. Ebbesen, and J. M. Gibson. Exceptionally high young's modulus observed for individual carbon nanotubes. Nature, 381:678, 1996.

2. A. Thess, R. Lee, P. Nikolaev, H. Dai, P. Petit, J. Robert, C. Xu, Y. H. Lee, S. G. Kim, A. G. Rinzler, D. T. Colbert, G. E. Scuseria, D. Tomanek, J. E. Fischer, and R. E. Smalley. Crystalline ropes of metallic carbon nanotubes. Science, 273:483, 1996.

3. J. W. G. Wildoer, L. C. Venema, A. G. Rinzler, R. E. Smalley, and C. Dekker. Electronic structure of atomically resolved carbon nanotubes. Nature, 391:59, 1998.

4. T. W. Odom, J. L. Huang, P. Kim, and C. M. Lieber. Atomic structure and electronic properties of single-walled carbon nanotubes. Nature, 391:62, 1998.

5. M. Pack, R. Figueiredo, B. Gojman, N. Mehta, E. Rachlin, D. Rizzo. Novel designs for nano-scale inductors. 2004

6. S. Iijima. Helical microtubules of graphite carbon. Nature, 354:56, 1991.

7. M. Endo, M. S. Dresselhaus. Carbon fibers and carbon nanotubes. 2002.

8. M. S. Dresselhaus, G. Dresselhaus, and R. Saito. Physics of carbon nanotubes. Carbon, 33:883, 1995.

9. T. W. Ebbesen, and P. M. Ajayan. Large-scale synthesis of carbon nanotubes. Nature, 358:220, 1992.

10. T. Guo, P. Nikolaev, A. Thess, D. T. Colbert and R. E. Smalley. Catalytic growth of single-walled manotubes by laser vaporization. Chem. Phys. Lett., 243:49, 1995.

11. M. José-Yacamán, M.Miki-Yoshida, L. Rendón, J. G. Santiesteban. Catalytic growth of carbon microtubules with fullerene structure. Appl. Phys. Lett., 62:657, 1993.

12. R. L. Vander Wal. Fe-catalyzed single-walled carbon nanotube synthesis within a flame environment. Combust. Flame, 130:37, 2002.

13. <http://en.wikipedia.org/wiki/Image:CNTnames.png>

14. <http://www6.ufrgs.br/lacer/gmn/imagens/nano1.jpg>

15. D. Pantarotto, J. Briand, M. Prato, A. Bianco. Translocation of bioactive peptides across cell membranes by carbon nanotubes. Chem. Comm. 16, 2004.

16. D. Pantarotto, R. Singh, D. McCarthy, M. Erhardt, J. Priand, M. Prato, K. Kostarelos, A. Bianco. Functionalized carbon nanotubes for plasmid DNA gene delivery. Angew. Chem., 43:5242, 2004

17. S. Kam, T. C. Jessop, P. A. Wender, H. Dai. Nanotube molecular transporters: internalization of carbon nanotube-protein conjugates into mammalian cells. J. Am. Chem. Soc. 126:6850, 2004.

18. Q. Lu, J. M. Moore, G. Huang, A. S. Mount, A. M. Rao, L. L. Larcom, P. C. Ke. RNA polymer translocation with single-walled carbon nanotubes. Nano Lett., 4:2473, 2004.

19. J. Chen, M. A. Hamon, H. Hu, Y. Chen, A. M. Rao, P. C. Eklund, R. C. Haddon. Solution properties of single-walled carbon nanotubes. Science, 282:95, 1998.

20. S. M. Bachilo, M. S. Strano, C. Kittrell, R. H. Hauge, R. E. Smalley, R. B. Weisman. Structure-assigned optical spectra of single-walled carbon nanotubes. Science, 298:2361, 2002.

21. N. W. S. Kam, Z. Liu, H. J. Dai. Functionalization of carbon nanotubes via cleavable disulfide bonds for efficient intracellular delivery of siRNA and protein gene silencing. J. Am. Chem. Soc., 127:12492, 2005.

22. N. W. S. Kam, H. J. Dai. Carbon nanotubes as intracellular protein transporters: generality and biological functionality. J. Am. Chem. Soc., 127:6021, 2005.

23. M. J. O'Connell, S. M. Bachilo, C. B. Huffman, V. C. Moore, M. S. Strano, E. H. Haroz, K. L. Rialon, P. J. Boul, W. H. Noon, C. Kittrell, J. Ma, R. H. Hauge, R. B. Weisman, R. E. Smalley. Band gap fluorescence from individual single-walled carbon nanotubes. Science, 297:593, 2002.

24. N. W. S. Kam, M. O'Connell, J. A. Wisdom, H. J. Dai. Carbon nanotubes as multifunctional biological transporter and near-infrared agents for selective cancer cell destruction. Proc. Natl. Acad. Sci. USA, 102:11600, 2005.

25. D. A. Heller, E. S. Jeng, T. K. Yeung, B. M. Martinez, A. E. Moll, J. B. Gastala, M .S. Strano. Optical detection of DNA conformational polymorphism on single-walled carbon nanotubes. Science, 311:508, 2006.

26. K. Kostarelos, L. Lacerda, G. Pastorin, W. Wu, S. Wieckowski, J. Luangsivilay, S. Godefroy, D. Pantarotto, J. Briand, S. Muller, M. Prato, A. Bianco. Cellular uptke of functionalized carbon nanotbes is independent of functional group and cell type. Nature nanotechnology, 2:108, 2007

27. A. V. Eletskii, B. M. Smirnov. Fullerenes and carbon structures. Phys-Usp., 38:935, 1995.

28. V. I. Sokolov, I. V. Stankevich. The fullerenes - new allotropic forms of carbon: molecular and electronic structure, and chemical properties. Russ Chem Rev., 62:419, 1993.

29. R. F. Curl, R. E. Smalley. Probing C_{60}. Science, 242:1017, 1988.

30. R. D. Johnson, G. Meijer, D. S. Bethune. C60 has icosahedral symmetry. J. Am. Chem. Soc. 112:8983, 1990.

31. D. R. McKenzie, C. A. Davis, D. J. Cockayne, D. A. Muller, A. M. Vassallo. The structure of the C70 molecule. Nature, 355:622, 1992.

32. <http://sbchem.sunysb.edu/msl/c60f.jpg>

33. <http://sbchem.sunysb.edu/msl/c70c.jpg>

34. L. L. Dugan, D. M. Turetsky, C. Du. Carboxyfullerenes as neuroprotective agents. Proc. Natl. Acad. Sci. U. S. A. 94:9434, 1997.

35. S. H. Friedman, D. L. DeCamp, R. P. Sijbesma, G. Srdanov, F. Wudl, G. L. Kenyon. Inhibition of the HIV-1 Protease by fullerene derivatives: model building studies and experimental verification. J. Am. Chem. Soc. 115:6506, 1993.

36. R. Sijbesma, G. Srdanov, F. Wudl, J. A. Castoro, C. Wilkins, S. H. Friedman, D. L. DeCamp, G. L. Kenyon. Synthesis of a fullerene derivative for the inhibition of HIV enzymes. J. Am. Chem. Soc. 115:6510, 1993.

37. N. Gharbi, M. Pressac, M. Hadchouel, H. Szwarc, S. R. Wilson, F. Moussa, Nano Lett. 2005, 5, 2578-2585.

38. T. Wharton, L. J. Wilson. Toward fullerene-based X-ray contrast agents: design and synthesis of non-ionic, highly-iodinated derivatives of C_{60}. Tetrahedron Lett. 43:561, 2002,.

39. J. M. Ashcroft, D. A. Tsyboulaski, K. B. Hartman, T. Y. Zakharian, J. W. Marks, R. B. Weisman, M. G. Rosenblum, L. J. Wilson. Fullerene (C_{60}) immunoconjugates: interaction of water-soluble C_{60} derivatives with the murine anti-gp240 melanoma antibody**.** Chem. Commun., 3004, 2006.

40. K. C. Hwang, D. Mauzerall. Photoinduced electron transport across a lipid bilayer mediated by C_{70}. Nature, 361:138, 1993.

41. S. Niu, D. Mauzerall. Fast and Efficient Charge Transport across a Lipid Bilayer Is Electronically Mediated by C_{70} Fullerene Aggregates. J. Am. Soc. Chem., 118:5791, 1996.

42. S. Foley, C. Crowley, M. Smaihi, C. Bonfils, B. F. Erlanger, P. Seta, C. Larroque. Cellular localization of a water-soluble fullerene derivative. Biochemical and Biophysical Research Communications. 294:116, 2002.

43. <http://probes.invitrogen.com/resources/education/tutorials/2Spectra/player.html>

44. L. Stryer. Fluorescence energy transfer as a spectroscopic ruler. Annu Rev Biochem, 47:819, 1978.

45. <http://meds.queensu.ca/qcri/flow/GScm_r11_c2.fret.png>

46. A. A. Shvedova, E. R. Kisin, R. Mercer, A. R. Murray, V. J. Johnson, A. I. Potapovich, Y. Y. Tyurina, O. Gorelik, S. Arepalli, D. S. Berry, A. F. Hubbs, J. Antonini, D. E. Evans, B. Ku, D. Ramsey, A. Maynard, V. E. Kagan, V. Castranova, P. Baron. Unusual inflammatory and fibrogenic pulmonary responses to single-walled carbon nanotubes in mice. Am. J. Physiol Lung Cell Mol. Physiol., 289:L698, 2005.

47. Z. Li, T. Hulderman, R. Salmen, R. Chapman, S. S. Leonard, S. Young, A. Shvedova, M. I. Luster, P. P. Simeonova. Cardiovascular effects of pulmonary exposure to single-wall carbon nanotubes. Environmental health perspectives. 115:377, 2007.

48. <http://www.sciencenews.org/articles/20050319/fob1.asp>

49. G. Oberdörster, A. Maynard, K. Donaldson, V. Castranova, J. Fitzpatrick, K. Ausman, J. Carter, B. Karn, W. Kreyling, D. Lai, S. Olin, N. Monteiro-Riviere, D. Warheit, H. Yang. Principles for characterizing the potential human health effects from exposure to nanomaterials: elements of a screening strategy. Particle & Fibre toxicology. 2:8, 2005.

50. G. Oberdörster, Z. Sharp, V. Atudorei, A. Elder, R. Gelein, W. Kreyling, C. Cox. Translocation of inhaled ultrafine particles to the brain. Inhalation toxicology, 16:437, 2004

51. M. J. O'Connell, S. M. Bachilo, C. B. Huffman, V. C. Moore, M. S. Strano, E. H. Haroz, K. L. Rialon, P. J. Boul, W. H. Noon, C. Kittrell, J. Ma, R. H. Hauge, R. B. Weisman and R. E. Smalley. Band Gap Fluorescence from Individual Single-Walled Carbon Nanotubes. Science, 297:593, 2002

52. K. Yurekli, C. A. Mitchell and R. Krishnamoorti. Small-Angle Neutron Scattering from Surfactant-Assisted Aqueous Dispersions of Carbon Nanotubes. J. Am. Chem. Soc., 126:9902, 2004,.

53. M. F. Islam, E. Rojas, D. M. Bergey, A. T. Johnson and A. G. Yodh. High Weight Fraction Surfactant Solubilization of Single-Wall Carbon Nanotubes in Water. Nano Lett., 3:269, 2003.

54. M. J. O'Connell, P. Boul, L. M. Ericson, C. Huffman, Y. Wang, E. Haroz, C. Kuper, J. Tour, K. D. Ausman and R. E. Smalley. Reversible water-solubilization of single-walled carbon nanotubes by polymer wrapping. Chem. Phys. Lett., 342:265, 2001.

55. M. Zheng, A. Jagota, E. D. Semke, B. A. Diner, R. S. McLean, S. R. Lustig, R. E. Richardson and N. G. Tassi. DNA-assisted dispersion and separation of carbon nanotubes. Nat. Mater., 2:338, 2003.

56. G. R. Dieckmann, A. B. Dalton, P. A. Johnson, J. Razal, J. Chen, G. M. Giordano, E. Munoz, I. H. Musselman, R. H. Baughman and R. K. Draper. Controlled Assembly of Carbon Nanotubes by Designed Amphiphilic Peptide Helices. J. Am. Chem. Soc., 125:1770, 2003.

57. Jorio, A.; Souza, A. G.; Dresselhaus, G.; Dresselhaus, M. S.; Swan, A. K.; Unlu, M. S.; Goldberg, B. B.; Pimenta, M. A.; Hafner, J. H.; Lieber, C. M.; Saito, R. G-band resonant Raman study of 62 isolated single-wall carbon nanotubes. Phys. Rev. B 2002, 65

.58. F. Zhang, Y. Fang. Nanostructure Origins of C60 Fluorescence in Pyridine. J. Phys. Chem. B 110:9022, 2002.